Article

Current Biology

ADF/Cofilin Accelerates Actin Dynamics by Severing Filaments and Promoting Their Depolymerization at Both Ends

Graphical Abstract

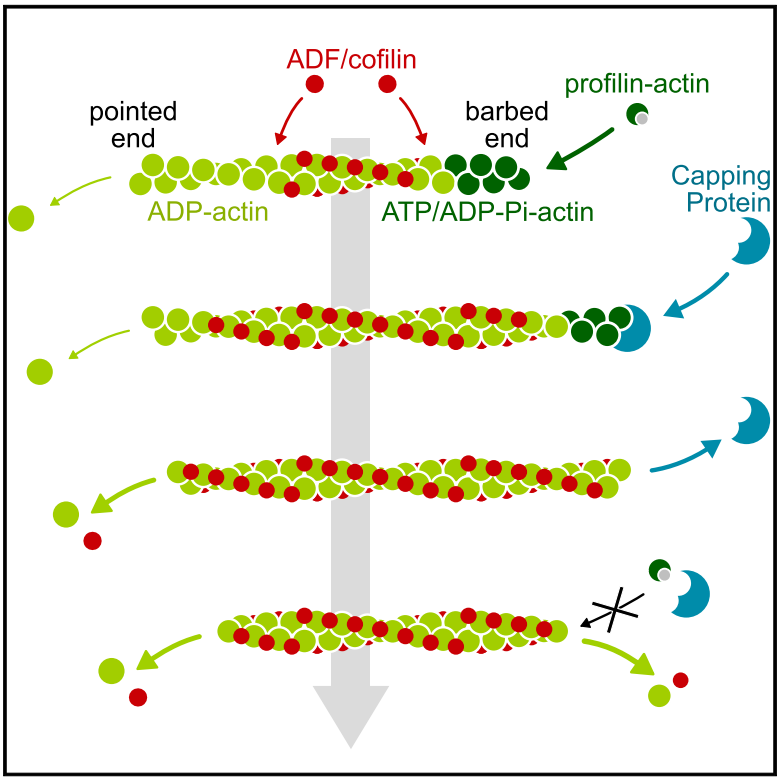

Highlights

- ADF/cofilin domains grow symmetrically and sever mostly at their pointed-end border
- Pointed-end depolymerization is accelerated by ADF/cofilin saturation
- ADF/cofilin domains reach capped barbed ends and rapidly uncap them
- ADF/cofilin-saturated barbed ends depolymerize and are hard to cap or re-elongate

Authors

Hugo Wioland, Berengere Guichard, Yosuke Senju, Sarah Myram, Pekka Lappalainen, Antoine Jégou, Guillaume Romet-Lemonne

Correspondence

antoine.jegou@ijm.fr (A.J.), romet@ijm.fr (G.R.-L.)

In Brief

Wioland et al. monitor the action of ADF/cofilin isoforms on individual actin filaments and characterize the reactions leading to filament disassembly. ADF/cofilin-saturated filaments differ greatly from bare filaments, as their barbed ends can hardly stop depolymerizing. This situation can arise from severing or from a synergy with capping protein.

Wioland et al., 2017, Current Biology *27*, 1956–1967
July 10, 2017
http://dx.doi.org/10.1016/j.cub.2017.05.048

CellPress

CellPress

Current Biology
Article

ADF/Cofilin Accelerates Actin Dynamics by Severing Filaments and Promoting Their Depolymerization at Both Ends

Hugo Wioland,[1] Berengere Guichard,[1] Yosuke Senju,[2] Sarah Myram,[1] Pekka Lappalainen,[2] Antoine Jégou,[1,*] and Guillaume Romet-Lemonne[1,3,*]
[1]Institut Jacques Monod, CNRS, Université Paris Diderot, 75013 Paris, France
[2]Institute of Biotechnology, University of Helsinki, P.O. Box 56, 00014 Helsinki, Finland
[3]Lead Contact
*Correspondence: antoine.jegou@ijm.fr (A.J.), romet@ijm.fr (G.R.-L.)
http://dx.doi.org/10.1016/j.cub.2017.05.048

SUMMARY

Actin-depolymerizing factor (ADF)/cofilins contribute to cytoskeletal dynamics by promoting rapid actin filament disassembly. In the classical view, ADF/cofilin sever filaments, and capping proteins block filament barbed ends whereas pointed ends depolymerize, at a rate that is still debated. Here, by monitoring the activity of the three mammalian ADF/cofilin isoforms on individual skeletal muscle and cytoplasmic actin filaments, we directly quantify the reactions underpinning filament severing and depolymerization from both ends. We find that, in the absence of monomeric actin, soluble ADF/cofilin can associate with bare filament barbed ends to accelerate their depolymerization. Compared to bare filaments, ADF/cofilin-saturated filaments depolymerize faster from their pointed ends and slower from their barbed ends, resulting in similar depolymerization rates at both ends. This effect is isoform specific because depolymerization is faster for ADF- than for cofilin-saturated filaments. We also show that, unexpectedly, ADF/cofilin-saturated filaments qualitatively differ from bare filaments: their barbed ends are very difficult to cap or elongate, and consequently undergo depolymerization even in the presence of capping protein and actin monomers. Such depolymerizing ADF/cofilin-decorated barbed ends are produced during 17% of severing events. They are also the dominant fate of filament barbed ends in the presence of capping protein, because capping allows growing ADF/cofilin domains to reach the barbed ends, thereby promoting their uncapping and subsequent depolymerization. Our experiments thus reveal how ADF/cofilin, together with capping protein, control the dynamics of actin filament barbed and pointed ends. Strikingly, our results propose that significant barbed-end depolymerization may take place in cells.

INTRODUCTION

Actin filament networks in cells undergo dynamic assembly, disassembly, and reorganization, exchanging subunits with a pool of cytoplasmic actin monomers that needs to be continuously regenerated [1, 2]. Therefore, the disassembly of "aged" actin filaments to produce assembly-competent monomers is a vital process in all eukaryotic cells. The members of actin-depolymerizing factor (ADF)/cofilin family proteins are the most conserved and essential proteins accelerating filament disassembly in cells [3, 4]. Inhibition of ADF/cofilin is consequently lethal at the embryonic stage and severely affects the morphology and actin-dependent functions of single cells [5, 6]. Moreover, misregulation of ADF/cofilin activity is linked to several pathologies, and ADF/cofilin are overexpressed in a number of tumor cells [7]. Whereas unicellular organisms typically express only a single ADF/cofilin isoform, multicellular organisms typically harbor several tissue-specific ADF/cofilin isoforms. In mammals, these are the ubiquitously expressed cofilin-1, neuron/epithelium-specific ADF, and muscle-specific cofilin-2 [8, 9].

ADF/cofilin are small, globular proteins that bind both monomeric (G-actin) and filamentous actin (F-actin), with a preference for ADP-bound actin subunits [10–13]. In actin filaments, ADF/cofilin bind between longitudinal neighbors in a cooperative manner [14, 15], leading to the formation of ADF/cofilin domains [13, 16, 17]. These domains modify locally the conformation and mechanical properties of the actin filament [18–21]. Whereas ADF/cofilin saturated filaments are stable, partially decorated filaments are severed at domain boundaries [13, 22]. The global severing activity of ADF/cofilin has been quantified [23, 24], although the kinetic rates of the reactions underlying ADF/cofilin activity have never been measured. Simple questions such as "what is the growth rate of a domain?" or "how rapidly does a domain sever a filament?" are still unanswered.

The globally accepted doctrine of actin dynamics in cells is based on treadmilling, the regime where filament barbed ends (BEs) grow while pointed ends (PEs) depolymerize [25]. The disassembly of filaments is thus thought to result from the blocking of barbed-end elongation by capping proteins (CPs) and depolymerization from the pointed ends. In this view, the enhancement of disassembly by ADF/cofilin could result from severing only, which multiplies the number of depolymerizing

pointed ends [26], or include an additional enhancement of pointed-end depolymerization [25]. Bulk solution assays have reported that ADF/cofilin increased the steady-state concentration of G-actin and accelerated filament treadmilling, leading to the proposal that ADF/cofilin accelerates pointed-end disassembly 25-fold [11]. This proposal has been contradicted by single-filament assays reporting a slow pointed-end depolymerization in the presence of ADF/cofilin [27].

The relative contributions of severing and depolymerization in ADF/cofilin-induced disassembly remain unclear today. We note that the comparison of data from different experiments is limited by the use of different ADF/cofilin isoforms from different species and by the use of different pH conditions, which greatly affect the activity of ADF/cofilin [28]. In fact, some studies specifically used a low pH in order to limit disassembly and observe filaments more easily [29].

Here, with a single-filament approach based on microfluidics, we fully quantified the binding (Figure 1), severing (Figure 2), and depolymerizing activities (Figures 3, 4, 5, and 6) of ADF/cofilin on actin filaments. We used all three mammalian isoforms of ADF/cofilin at pH 7.8. We revealed that pointed-end depolymerization is enhanced by ADF/cofilin, but not to the extent predicted by bulk assays (Figure 4), and discovered that ADF/cofilin favors barbed-end depolymerization through two distinct mechanisms. The first mechanism consists of a direct targeting of bare filament barbed ends, which is avoided when ATP-actin is present (Figure 3). The second mechanism consists of preventing the barbed ends of ADF/cofilin-saturated filaments from elongating or becoming capped (Figure 5), thus promoting barbed-end depolymerization in physiological conditions (Figure 6), contrary to the general consensus.

RESULTS

A Single-Filament Approach Based on Microfluidics

We monitored the different activities of ADF/cofilin on individual filaments, using a combination of live fluorescence microscopy and microfluidics that we have developed over the past years [30]. This allowed us to accurately observe large numbers of filaments anchored to the coverslip by one end only, while successively exposing them to controlled flows of different protein solutions. We worked at a pH of 7.8, with α-skeletal muscle actin (skeletal actin, from rabbit) as well as β/γ cytoplasmic actin (cytoplasmic actin, from bovine spleen), and with all three mammalian isoforms of ADF/cofilin: ADF, cofilin-1, and cofilin-2, collectively referred to as "ADF/cofilin."

The reaction rates that we present here were not affected by flow rates (Figure S1A). The tensile force exerted by the flowing solution on the actin filaments [31] remained in the range of a few pN, well below the forces reported to impede ADF/cofilin activity [32].

A typical experiment was carried out as shown in Figure 1. Filaments of ADP-actin were formed in a microchamber, with only one end anchored to the surface. Using solutions containing 15% labeled and unlabeled actin allowed us to generate either uniformly labeled filaments or filaments containing long unlabeled segments (Figure 1D) [31, 33]. Filaments were then exposed to a solution of fluorescent mCherry- or eGFP-fusion cofilin-1 or cofilin-2, domains of which could be seen growing on the filament (Figure 1). The impact of cofilin labeling on domain dynamics was found to be very mild and taken into account (Figure S1). Severing events were also monitored and quantified (Figure 2). The depolymerization of the free (non-anchored) filament ends was measured using unlabeled ADF/cofilin, i.e., with ADF as well as cofilin-1 and cofilin-2 (Figures 3, 4, 5, and 6).

Cofilin Domains Grow Symmetrically and Sever Filaments Asymmetrically

We first monitored the appearance of cofilin domains, which emerged uniformly on ADP-actin filaments over time (Movie S1). To quantify domain appearance, we measured the decrease in the number of the 10-μm-long filament segments that did not exhibit any detectable cofilin domain, over time (Figure S2A). Exponential fits of these curves yielded the domain appearance rates, which scale linearly with cofilin concentration over the explored range (Figure 1E). We found that cofilin-2 domains form faster compared to cofilin-1 domains, and that domains form more rapidly on skeletal actin than on cytoplasmic actin.

To characterize domain growth dynamics, we tracked the position of their edges (see STAR Methods) and found that they progressed linearly over time (Figure S2B), at the same velocity in both directions (Figure 1F). By fitting linearly this velocity as a function of concentration, we determined the on- and off-rate constants for cofilin at domain edges (Figures 1G and 1J). Cooperativity is very strong: we find that the on-rate for cofilin binding to the edge of a domain (Figure 1G) is approximately five orders of magnitude higher than the effective domain appearance rate (Figure 1E; which itself is certainly lower than the on-rate of the first isolated cofilin). Overall, cofilin domains appeared more slowly but grew faster on cytoplasmic actin than on skeletal actin filaments.

To monitor the growth of very small domains just after nucleation, we measured the increase in fluorescence and found that domains grew at a constant rate as soon as they were composed of a few cofilin molecules (Figure S2C). Consistent with earlier observations [13], cofilin domains are very stable, with almost no cofilin departing from the center of the domain. In order to quantify this, we performed a chase experiment, where we monitored the binding of labeled cofilin on a filament saturated with unlabeled ADF/cofilin (Figures 1H, 1I, and S2E). We found that cofilin departs from within a domain at a rate more than four orders of magnitude lower than from the edges of a domain.

In order to obtain reliable statistics on severing events, we generated a large number of cofilin domain boundaries on actin filaments. We proceeded either by rapidly generating cofilin domains and then exposing filaments to buffer alone (Figure 2A; Movie S2) or by continuously exposing filaments to low amounts of cofilin (Figures 2C and 2D). In the majority of cases, severing events took place at the pointed-end side of a cofilin domain, regardless of which end of the filament was anchored to the surface (Figure 2B). This result is consistent with recent observations from two other groups [24, 34].

In order to quantify the severing rate, we have plotted the fraction of growing cofilin domains that have not yet had a severing event as a function of the age of each domain (see STAR Methods). We find that after a lag period, this survival fraction is

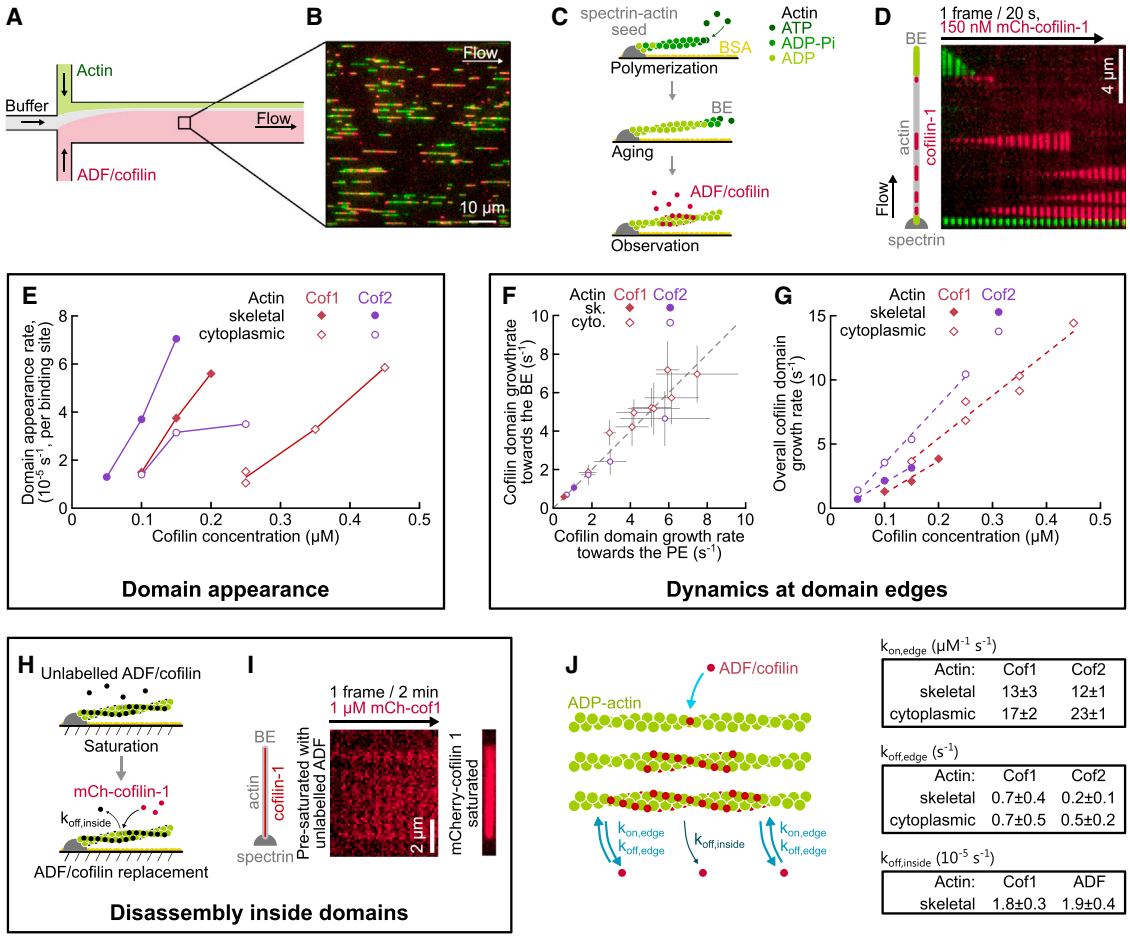

Figure 1. Appearance and Growth Dynamics of Cofilin Domains on ADP-Actin Filaments in a Microfluidic Chamber

(A–D) Description of the experiment.

(A) Sketch of the microfluidic setup, showing the situation where the incoming flow of the ADF/cofilin solution dominates.

(B) Typical field of view showing Alexa 488-labeled skeletal actin filaments (green) covered with mCherry-cofilin-1 (red), observed by total internal reflection fluorescence (TIRF) microscopy. Only one-fourth of the full field of view is shown, for clarity. See also Movie S1.

(C) Typical sequence of our experiments. Filaments are grown from surface-anchored spectrin-actin seeds and aged for 15 min with a solution of G-actin at critical concentration in order to become fully ADP-actin. They are then exposed to a solution of ADF/cofilin. Filaments are monitored throughout the process. Solutions flow from left to right.

(D) Time-lapse record showing the binding of 150 nM mCherry-cofilin-1 (red) to a large segment of unlabeled actin. Segments of Alexa 488-actin (green) were polymerized close to the barbed and pointed ends to locate filaments.

(E) Appearance rate of eGFP-cofilin-1 and eGFP-cofilin-2 domains onto unlabeled skeletal and cytoplasmic actin, computed per cofilin-binding site on the side of the filament (N = 9–30 filaments). See also Figure S2A.

(F and G) Dynamics at cofilin domain edges.

(F) eGFP-cofilin-1 and eGFP-cofilin-2 domains on skeletal and cytoplasmic actin grow as fast toward the pointed end as toward the barbed end (the dashed line represents equal velocities). Each dot corresponds to the mean over 5–39 domain edges from one experiment. Error bars indicate SD.

(G) Domain growth rates of eGFP-cofilin-1 and eGFP-cofilin-2 on unlabeled skeletal and cytoplasmic actin. Data points correspond to the median over 9–22 domains. Dashed lines are linear fits yielding the on-rate constant (slope) and off-rate constant (intercept) for cofilin at domain edges. Resulting values are in (J). See also Figure S2B.

(H and I) ADF/cofilin disassembly from within domains.

(H) Sketch of the experiment: filaments are first saturated with unlabeled ADF or cofilin-1. Binding of mCherry-cofilin-1 then reveals the amount of departed unlabeled ADF/cofilin.

(I) Time-lapse record of a filament pre-saturated with unlabeled ADF and exposed to 1 µM mCherry-cofilin-1, compared to an mCherry-cofilin-1-saturated filament displayed with identical contrast settings. See also Figure S2E.

(J) Summary of the ADF/cofilin assembly mechanism and corresponding rates.

See also Figures S1, S2, and S4.

well fitted by an exponential, yielding the severing-rate constant per domain (Figure 2D). Increasing the cofilin concentration reduced the duration of the lag period, indicating that this lag corresponds to a minimal domain size required for severing to occur. We estimated this minimal size to be approximately 100 subunits. We also found that severing per domain is globally faster on

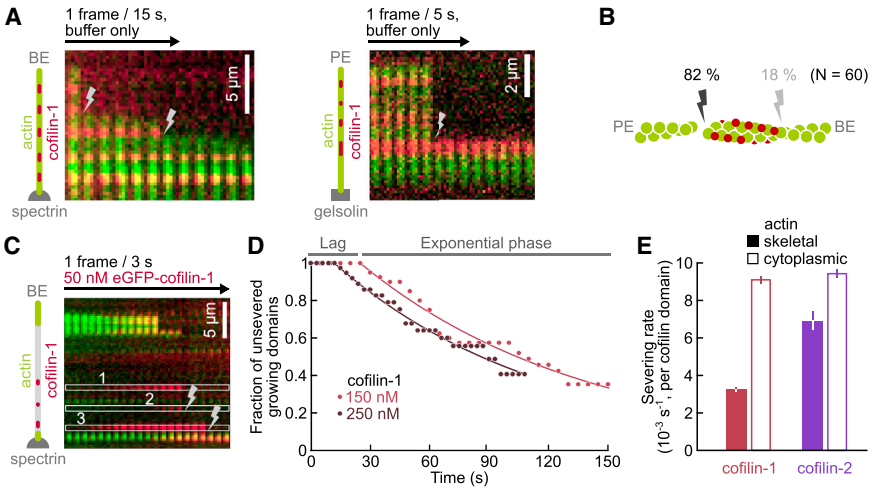

Figure 2. Characterization of Filament Severing by Cofilin Domains

(A and B) Localization of severing events with pre-formed cofilin domains (red) on labeled filaments (green).

(A) Time-lapse record showing severing of Alexa 488 skeletal actin filaments, anchored by their pointed end (left) or by their barbed end (right) and decorated by mCherry-cofilin-1 domains prior to imaging. Lightning bolt symbols indicate severing events. See also Movie S2.

(B) Fraction of severing events near domain edges happening toward the pointed or barbed end.

(C–E) Measurement of the severing rate from growing cofilin domains on unlabeled filament segments.

(C) Time-lapse record showing the growth of three eGFP-cofilin-1 (50 nM) domains (numbered 1, 2, and 3) and severing events (lightning bolt symbols) on unlabeled skeletal actin.

(D) Surviving fraction of unsevered eGFP-cofilin-1 domains on unlabeled cytoplasmic actin (N = 40). Time t = 0 corresponds to the estimated nucleation time for each domain. The exponential fits (lines) yield the severing-rate constants.

(E) Severing-rate constants for growing eGFP-cofilin-1 and eGFP-cofilin-2 domains on unlabeled skeletal and cytoplasmic actin (N = 30–40; error bars result from the exponential fit of the data).

See also Figures S1 and S4.

cytoplasmic actin than on skeletal actin, and that cofilin-2 domains sever more frequently than cofilin-1 domains, especially on skeletal actin. Earlier studies have reported the global severing activity of ADF/cofilin without identifying domains [23, 24]. In order to compare our results to these studies, we performed numerical simulations integrating the rates we have measured for domain nucleation, growth, and severing (for more details, see STAR Methods), and found that our results are in good agreement with the published data (Figures S4A and S4B).

Together, these experiments reveal the rates of ADF/cofilin domain nucleation and elongation on skeletal and cytoplasmic actin filaments, and provide quantitative evidence that ADF/cofilin preferentially sever filaments at the pointed-end side of an ADF/cofilin domain. In the rest of this article, we investigate the behavior of filament ends in the presence of ADF/cofilin.

Free ADF/Cofilin in Solution Directly Targets Bare Filament Barbed Ends Containing ADP- and ADP-Pi- but Not ATP-Actin

When exposing ADP-actin filaments to cofilin in order to monitor domain formation and severing, we also noticed that barbed ends with no detectable cofilin domain depolymerized faster than expected (Figure 3A). We found that this faster barbed-end depolymerization increased strongly with the concentration of ADF/cofilin in the buffer, and that it was stronger for ADF and cofilin-2 than for cofilin-1 (Figure 3C). We found that this effect also took place in saturating phosphate conditions, when F-actin subunits are maintained in their ADP-Pi state (Figure 3D). When a cofilin domain was reached (Movie S3; arrowheads in Figure 3A), barbed-end depolymerization slowed down and matched the rate measured for saturated filaments (Figure 4). We verified that accelerated depolymerization was due to free ADF/cofilin in solution by transiently exposing depolymerizing filaments to ADF. In this experiment, depolymerization was enhanced only when ADF was present in solution (Figure 3B). These results indicate that ADF/cofilin in solution destabilizes bare actin filament barbed ends.

We then asked whether this destabilization was the result of ADF/cofilin interacting directly with the barbed face of the terminal subunit or with the last side-binding site near the barbed end (Figure 3F). Interaction with the terminal barbed face would only involve the "G-binding site" of ADF/cofilin, whereas side binding would also involve the "F-binding site" of ADF/cofilin [21, 35, 36]. We thus designed a K96A D98A mutant of cofilin-1, where the F-binding site is inactivated. As expected, this mutant bound only weakly to the side of actin filaments (Figure S3C). Despite a drastic defect in filament side-binding activity, the K96A D98A mutant induced barbed-end depolymerization with identical efficiency compared to wild-type cofilin-1 (Figure 3F). This result indicates that ADF/cofilin in solution destabilizes the terminal subunit by interacting directly with its barbed face, through its "G-binding site," which is still intact in the K96A D98A mutant.

In the presence of ATP-G-actin, filaments are expected to grow with an ADP-Pi-rich region near their barbed end, where ADF/cofilin does not bind [13]. We added ATP-G-actin in our experiment and confirmed this observation (Figure 3G). We also observed that the elongation rate was not affected by the presence of ADF/cofilin in solution (Figure 3H). We also added CP in solution, and found that the capping rate on elongating filaments was not affected by the presence of ADF/cofilin in solution (Figure 3I). These results show that free ADF/cofilin does not interact with ATP-actin at the barbed end. It thus seems that ATP-actin protects the barbed end from direct targeting by ADF/cofilin present in solution, allowing filaments to sustain elongation in the presence of ADF/cofilin.

ADF-Saturated Actin Filaments Depolymerize Faster, from Both Ends, Than Cofilin-Saturated Filaments

We saturated filaments, anchored to the coverslip surface by either their pointed or barbed end, with ADF/cofilin in order to

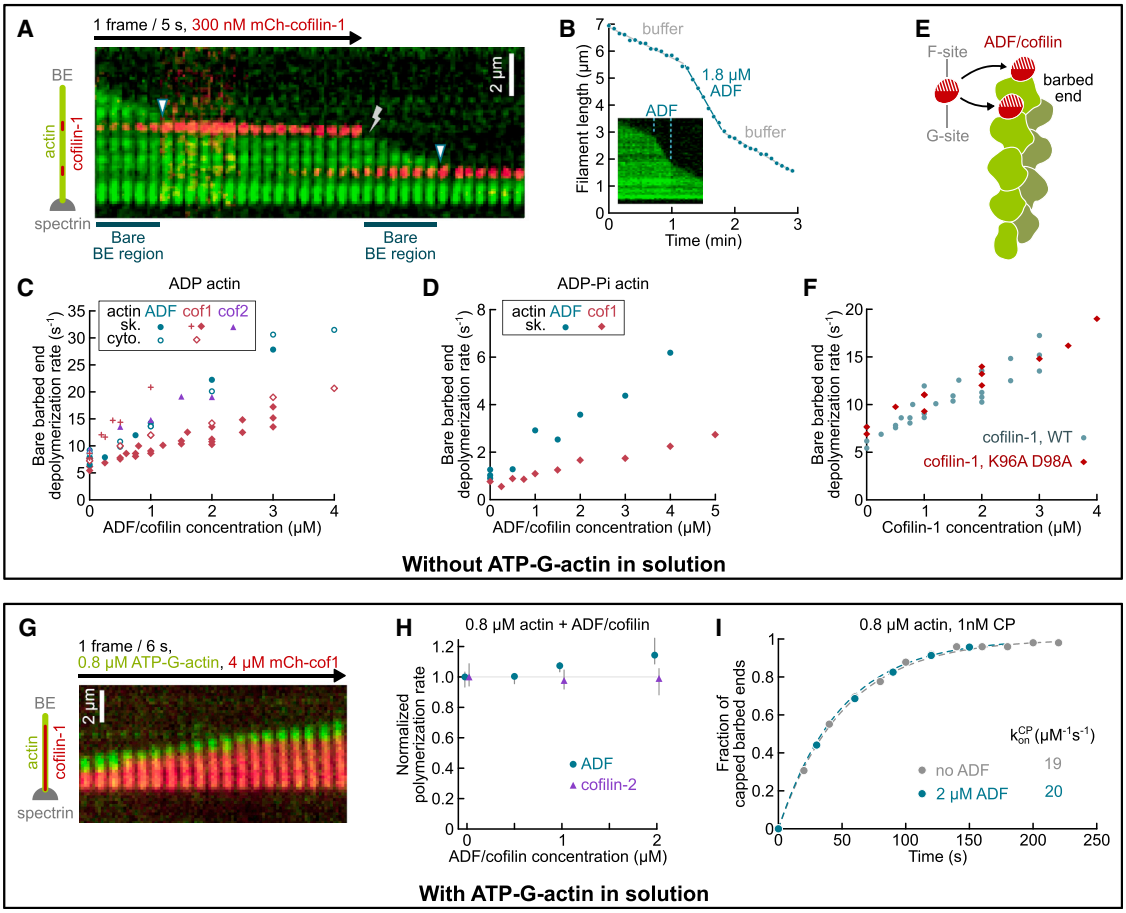

Figure 3. Free ADF/Cofilin Targets ADP- and ADP-Pi-Actin Barbed Ends but Not ATP-Actin Barbed Ends

(A–F) In the absence of ATP-G-actin, ADF/cofilin directly targets the bare BE to accelerate its depolymerization.

(A) Time-lapse record of an Alexa 488 skeletal actin filament (green) depolymerizing in the presence of 300 nM mCherry-cofilin-1 (red). The depolymerization rate is higher when no cofilin-1 domain is near the BE (see also Movie S3). Rapid depolymerization stops when the BE reaches a cofilin-1 domain (arrowheads), which slows down depolymerization (see Figure 4), and resumes when the domain severs off (lightning bolt symbol).

(B) A skeletal ADP-actin filament transiently exposed to 1.8 µM unlabeled ADF depolymerizes faster only when ADF is present in the solution. Inset: kymograph of the same Alexa 488 skeletal actin filament.

(C and D) Barbed-end depolymerization of labeled skeletal and cytoplasmic ADP- (C) and ADP-Pi-actin (D) as a function of the concentration of unlabeled ADF/cofilin in the solution. All data points in (C)–(F) were acquired with 100 mM KCl in order to slow down the formation of ADF/cofilin domains and allow us to make measurements at higher ADF/cofilin concentrations, except for plus symbols (+) in (C), which were acquired with our standard 50 mM KCl and are shown here for comparison (see also Figures S1F, S3A, and S3B). Each point represents the median over one experiment. N = 6–40 filaments.

(E) Model of ADF/cofilin binding to the BE. Only the G site is required to bind the very last subunit.

(F) The depolymerization rate of the skeletal actin BE is unaffected by K96A D98A mutations to the F site of unlabeled cofilin-1 (see also Figure S3C). Each point represents the median over N = 6–40 filaments. The data points for cofilin-1 wild-type (WT) are identical to the ones in (C).

(G–I) In the presence of ATP-G-actin, filaments polymerize and get capped regardless of ADF/cofilin concentration.

(G) Time-lapse record of an Alexa 488 skeletal actin filament (green) polymerizing in the presence of 4 µM mCherry-cofilin-1 (red). ATP- and ADP-Pi-actin near the barbed end prevent ADF/cofilin binding.

(H) Polymerization rate in the presence of 0.8 µM skeletal ATP-G-actin and varying concentrations of ADF and cofilin-2. Rates are normalized by the average rate measured in the absence of ADF/cofilin. Data points are median values and error bars indicate quartiles (N = 5–13 for ADF; N = 26–34 for cofilin-2).

(I) Capping (1 nM CP) of a population of growing skeletal actin (0.8 µM) filament barbed ends in the absence and presence of 2 µM ADF (N = 50 for each condition). The CP on-rate constants are determined by the exponential fits (dashed lines).

See also Figures S1, S3, and S4.

monitor the dynamics of their free ends. In each configuration, the filaments were exposed to buffer with no actin monomers, and depolymerization was observed and compared to control filaments (Figure 4). The depolymerization of saturated filaments was not affected by the presence of ADF/cofilin in solution (Figure S5).

Compared to bare actin filaments, ADF/cofilin-saturated filaments depolymerized more rapidly from their pointed ends and slower from their barbed ends (Figure 4B). As a result, both ends of ADF/cofilin-saturated filaments depolymerize at similar rates, the barbed end remaining slightly faster. Pointed-end depolymerization is increased approximately 3-fold for cofilin-1- and

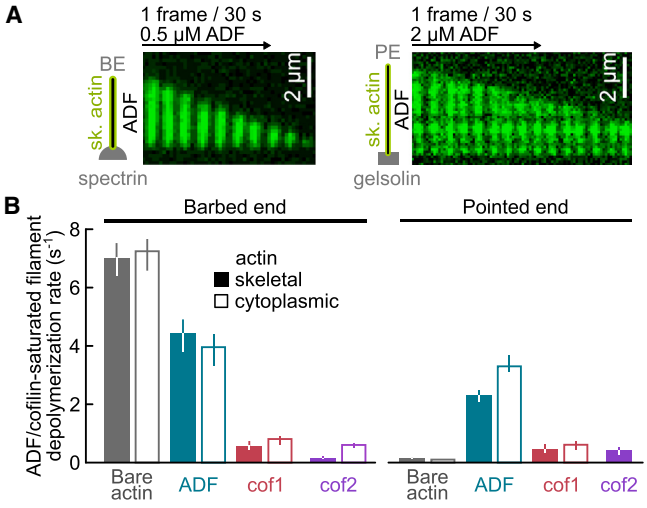

C

	Depolymerization rate (± SD, s^{-1})			
	Barbed end		Pointed end	
actin	skeletal	cytoplasmic	skeletal	cytoplasmic
bare filament	7.0 ± 0.6	7.3 ± 0.5	0.2 ± 0.1	0.1 ± 0.1
ADF-saturated	4.4 ± 0.6	4.0 ± 0.5	2.3 ± 0.2	3.3 ± 0.3
cofilin-1-saturated	0.6 ± 0.2	0.9 ± 0.1	0.5 ± 0.1	0.6 ± 0.2
cofilin-2-saturated	0.2 ± 0.1	0.6 ± 0.1	0.4 ± 0.1	-

Figure 4. Depolymerization of ADF/Cofilin-Saturated Filaments Is Slower at the BE and Faster at the PE, Compared to Bare Filaments

(A) Time-lapse record of Alexa 488 actin filaments saturated with unlabeled ADF, depolymerizing from their BE (left) or PE (right). Filaments were saturated with ADF prior to imaging, and ADF was kept in the background to maintain ADF saturation of the filaments.

(B) BE and PE depolymerization rates measured on ADP-actin filaments anchored by spectrin-actin seeds and gelsolin, respectively. Values are medians measured on populations of (from left to right) N = (BE) bare: 406, 117; ADF: 15, 21; cof1: 19, 13; cof2: 19, 8; and (PE) bare: 158, 33; ADF: 20, 33; cof1: 32, 16; cof2: 23. Error bars indicate quartiles.

(C) Table summarizing the depolymerization rates shown in (B). All rates were obtained by first saturating filaments with unlabeled ADF/cofilin. Depolymerization was then monitored, keeping 0.5–2 μM ADF/cofilin in the solution to prevent filament severing. Rates do not depend on ADF/cofilin concentration in the buffer during depolymerizaton (Figure S5).

See also Figures S1E, S4, and S5.

cofilin-2-saturated skeletal actin filaments and 12-fold for ADF-saturated skeletal actin filaments. Cofilin-saturated filaments are very stable compared to ADF-saturated or bare filaments: considering both ends, a cofilin-1-saturated skeletal actin filament in buffer will lose 1.1 ± 0.4 subunits per second, whereas an ADF-saturated filament will lose 6.7 ± 0.6 subunits/s and a bare filament will lose 7.2 ± 0.6 subunits/s. Cytoplasmic actin filaments follow the same trend, with slightly faster rates (Figure 4C).

These results indicate that ADF/cofilin alone, by modifying the conformation of the filaments they decorate, are sufficient to destabilize filament pointed ends. In contrast, the same filament conformation induced by ADF/cofilin decoration stabilizes filament barbed ends. The barbed ends of ADF/cofilin-saturated filaments nonetheless exhibit a significant depolymerization.

In order to compare our results to published reports of actin disassembly in bulk solution assays [9], we performed numerical simulations integrating the individual reaction rates that we have measured (see STAR Methods). Our computed curves show that our reaction rates account well for the global disassembly of actin filaments, measured in the absence of actin monomers (Figure S4C).

ADF/Cofilin-Saturated Filaments Depolymerize from Barbed Ends in the Presence of G-Actin, Profilin-Actin, and Capping Protein

We then asked whether ADF/cofilin-decorated barbed ends behaved like bare barbed ends with respect to elongation and capping, as is often assumed. To address this question, we exposed ADF/cofilin-saturated filaments to solutions containing CP or ATP-G-actin (Figure 5A). We first observed that these filaments continued to depolymerize at the same rate as in the absence of CP or monomeric actin (Figure 5B).

We next quantified the impact of ADF/cofilin saturation on the affinity of CP for the barbed end. This was achieved most accurately for ADF-saturated filaments because they exhibit rapid barbed-end depolymerization (Figure 4), but similar rates were also measured for cofilin (Figure S6). We found that the on-rate of CP on depolymerizing ADF-saturated filaments was decreased more than 50-fold compared to bare filaments (Figure 5C). We then quantified the off-rate of CP from ADF-saturated filament barbed ends, and found that it was 12-fold higher than from bare filaments (Figure 5D). Together, these results show that the affinity of CP for the barbed end is more than 600-fold lower when the filament is saturated with ADF.

We also observed that depolymerizing ADF-saturated filaments exposed to ATP-G-actin occasionally started elongating (Figure 5E). These new elongation phases exhibited the expected elongation rate based on ATP-G-actin concentration, confirming that actin monomers were not sequestered by ADF/cofilin. We measured the cumulative occurrence of these "rescues" for different actin concentrations (Figure 5F) and revealed that they occurred with a rate constant of approximately $4 \cdot 10^{-3}$ $\mu M^{-1} s^{-1}$ for cofilin-1-saturated filaments, which is more than three orders of magnitude below the on-rate constant for ATP-G-actin to a bare barbed end. The effect seems to be even more pronounced in the presence of profilin: ADF/cofilin-saturated filaments exposed to profilin-actin are rescued with a rate constant smaller than $1 \cdot 10^{-3}$ $\mu M^{-1} s^{-1}$ (Figure 5F).

Together, these results indicate that ADF/cofilin-saturated filaments are in a conformation that hinders barbed-end elongation and capping, and thus promotes barbed-end depolymerization.

Growing Barbed Ends Exposed to CP Eventually Become Decorated by ADF/Cofilin and Depolymerize

We next sought to determine whether such ADF/cofilin-decorated barbed-end depolymerization could contribute to actin dynamics in conditions occurring in cells. We first observed this situation as a result of severing events. Filaments growing in the presence of ADF/cofilin sever at ADF/cofilin domain boundaries, and 17% (N = 66) of these severing events generate an ADF/cofilin-saturated barbed end, which undergoes depolymerization (Figure 6A). This number is similar to what we measured for the severing of old ADP-actin filaments (Figure 2B). When monitoring

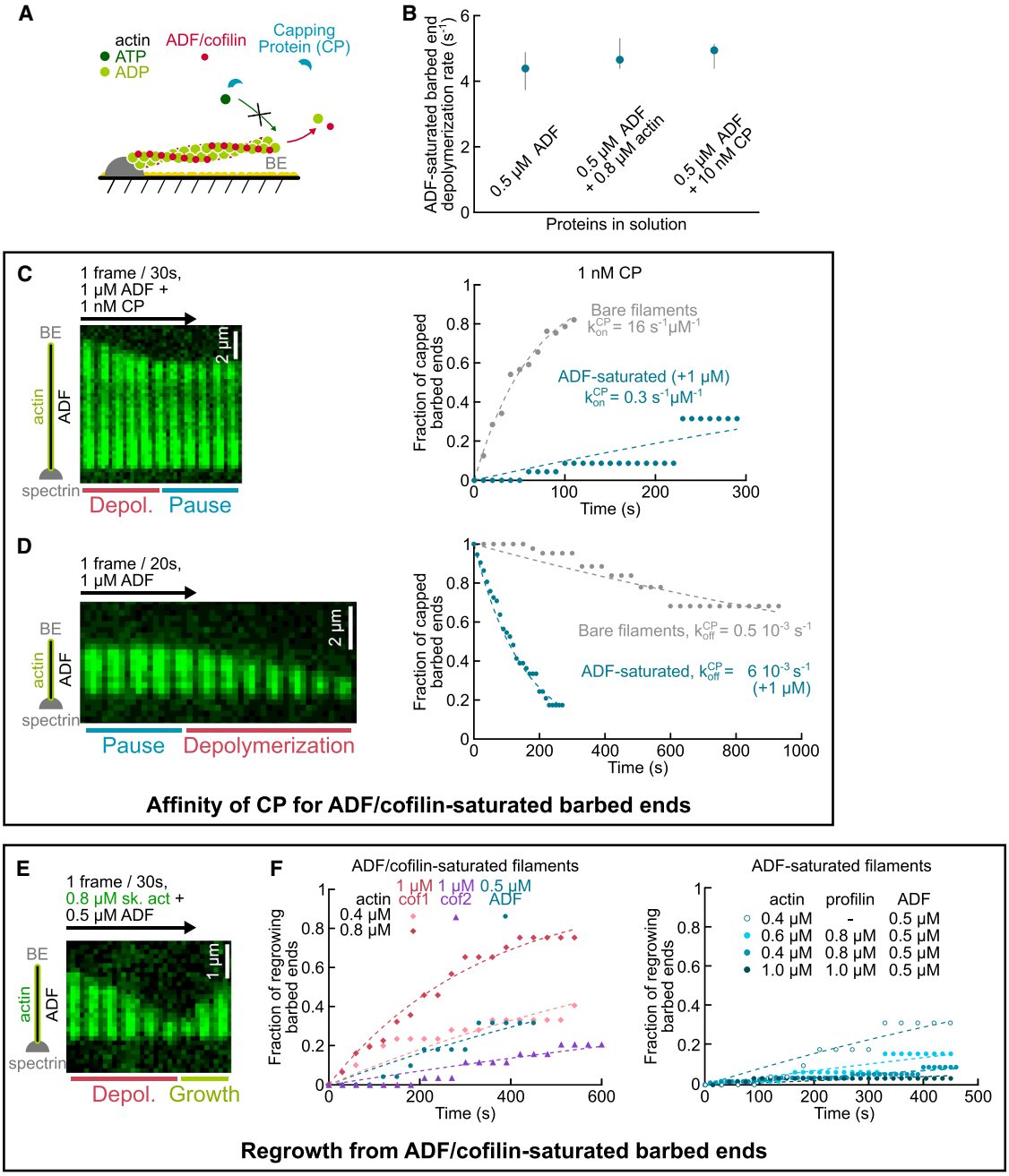

Figure 5. Saturation by ADF/Cofilin Greatly Hinders the Binding of Actin and CP to the Barbed End

(A) Sketch of the experiment. After saturation by ADF/cofilin, filaments are continuously exposed to a solution containing actin, ADF/cofilin, and CP.

(B) Depolymerization rate of ADF-saturated barbed ends (skeletal actin) in the presence and absence of 0.8 µM G-ATP-actin and 10 nM CP. Data points are median values, and error bars indicate quartiles (from left to right: N = 15, 10, 5).

(C and D) ADF/cofilin saturation reduces drastically the affinity of CP to the barbed end.

(C) Time-lapse record of an ADF-saturated filament depolymerizing in the presence of 1 µM ADF and 1 nM CP. The binding of CP to the barbed end pauses depolymerization. Occurrence of pauses during the depolymerization of populations of bare (N = 30) and ADF-saturated (N = 23) skeletal actin filaments exposed to 1 nM CP. The CP on-rate constants are determined by fitting the data with computed curves (dashed lines) and accounting for photo-induced pauses, which were minimal over this timescale (see STAR Methods).

(D) Time-lapse record of a capped ADF-saturated filament exposed to buffer containing 1 µM ADF. The onset of depolymerization indicates the departure of CP from the barbed end. Survival fractions of capped filaments for populations of bare (N = 46) and ADF-saturated (N = 43) skeletal actin filaments. The CP off-rate constants are determined by the exponential fits (dashed lines). See also Figure S6.

(E and F) ADF/cofilin-saturated filaments depolymerize in spite of ATP-G-actin.

(E) Time-lapse record of an ADF-saturated filament depolymerizing and repolymerizing while continuously exposed to 0.8 µM Alexa 488-actin and 0.5 µM ADF.

(legend continued on next page)

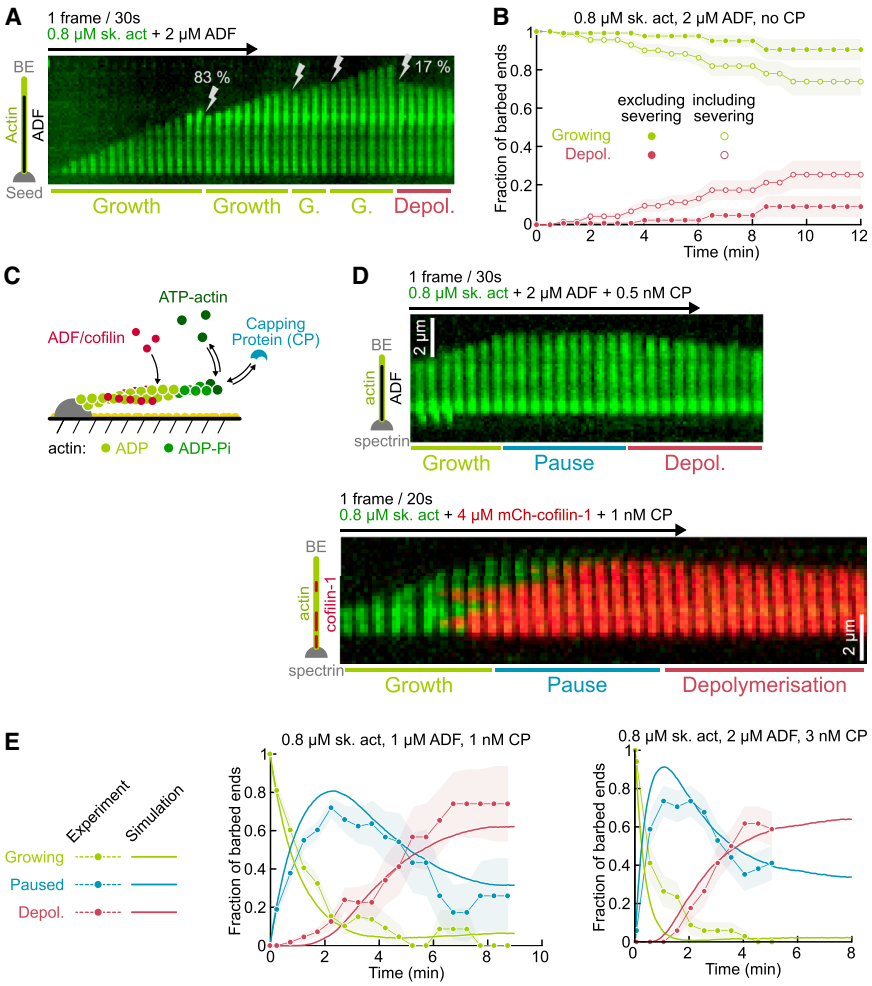

Figure 6. ADF/Cofilin and CP Cooperate to Induce Barbed-End Depolymerization

(A and B) Severing events can generate depolymerizing BEs.

(A) Time-lapse record of a filament polymerizing in the presence of 0.8 μM Alexa 488-actin and 2 μM ADF, showing four severing events, one of which induces filament depolymerization. Altogether, 17% (N = 66) of severing events result in barbed-end depolymerization.

(B) Fractions of a population of N = 133 filament BEs polymerizing and depolymerizing over time, in the presence of 0.8 μM Alexa 488-actin and 2 μM ADF.

(C–E) CP allows ADF/cofilin saturation and subsequent BE depolymerization.

(C) Sketch of the experiments. A solution of actin, ADF/cofilin, and CP is constantly injected into the microfluidic chamber. Filaments are monitored as they polymerize, get capped, and depolymerize.

(D) Time-lapse record showing the typical sequence of events leading to BE depolymerization: filaments polymerize until a CP binds the BE. ADF (top) or mCh-cofilin1 (bottom) then saturates the filament, releasing CP and inducing BE depolymerization. A solution of 0.8 μM Alexa 488-actin, 2 μM ADF (top) or 4 μM mCh-cofilin-1 (bottom), and 0.5 nM CP (top) or 1 nM CP (bottom) was constantly injected throughout the experiment.

(E) Fractions of populations of BEs growing, pausing, and depolymerizing while continuously exposed to 0.8 μM Alexa 488-actin, 1 μM ADF, and 1 nM CP (left) or 0.8 μM Alexa 488-actin, 2 μM ADF, and 3 nM CP 2 μM (right). Symbols indicate fractions determined from experiments, excluding severing events (N = 111 and 34, respectively; error bars indicate binomial SD). Solid lines correspond to simulations for a population of 10,000 filaments exposed to the same protein concentrations, computed using the reaction rates determined independently for capping, uncapping, rescues during depolymerization (Figure 5), and the saturation of filaments once they are capped (Figure S7A), with no adjustable parameter. See also Figures S7B–S7D.

See also Figure S7.

a population of filaments anchored by their pointed ends and exposed to a solution of ATP-G-actin and ADF, a moderate proportion of the observed barbed ends depolymerize over time as a result of these severing events (Figure 6B). If we exclude severing events, a small proportion of filaments (less than 10% over 12 min) switch from elongation to depolymerization, most likely because of near-end severing events that could not be resolved as such in our experiment.

In cells, elongating actin filaments are eventually capped by CP present in the cytoplasm. We thus repeated the same analysis, excluding severing events, for filaments continuously exposed to a solution containing CP, ATP-G-actin, and ADF (Figures 6C–6E and S7B–S7D). We found that, after a few minutes, most filaments are depolymerizing from their barbed ends. The time required to convert a population of growing barbed ends into mostly depolymerizing barbed ends depends mainly on the concentrations of CP and ADF/cofilin.

Using labeled cofilin, we observed that capping allows ADF/cofilin to decorate filaments up to their barbed ends (Figure 6D). This process typically takes 50–300 s, and is faster for higher ADF/cofilin concentrations (Figure S7A). Once the barbed end is decorated by ADF/cofilin, CP rapidly falls off and the barbed end starts depolymerizing. Using numerical simulations integrating the individual reaction rates that we have measured, we have computed (with no free parameter) the evolution of the filament population for different sets of protein concentrations. The computed curves are in good agreement with our experimental results (Figures 6E and S7B–S7D), confirming that the "cap-saturate-uncap" mechanism that we quantified is responsible for the observed barbed-end depolymerization (Figure 7, right).

(F) Fraction of different populations of ADF/cofilin-saturated filaments that have switched to elongation, over time exposed to skeletal ATP-G-actin and profilin. Left: saturation by all ADF/cofilin isoforms protects the barbed end from repolymerizing (N = 24–30). Right: profilin further delays the repolymerization of ADF-saturated barbed ends (N = 24–190). Dashed lines are exponential fits of the data.

See also Figures S5 and S6.

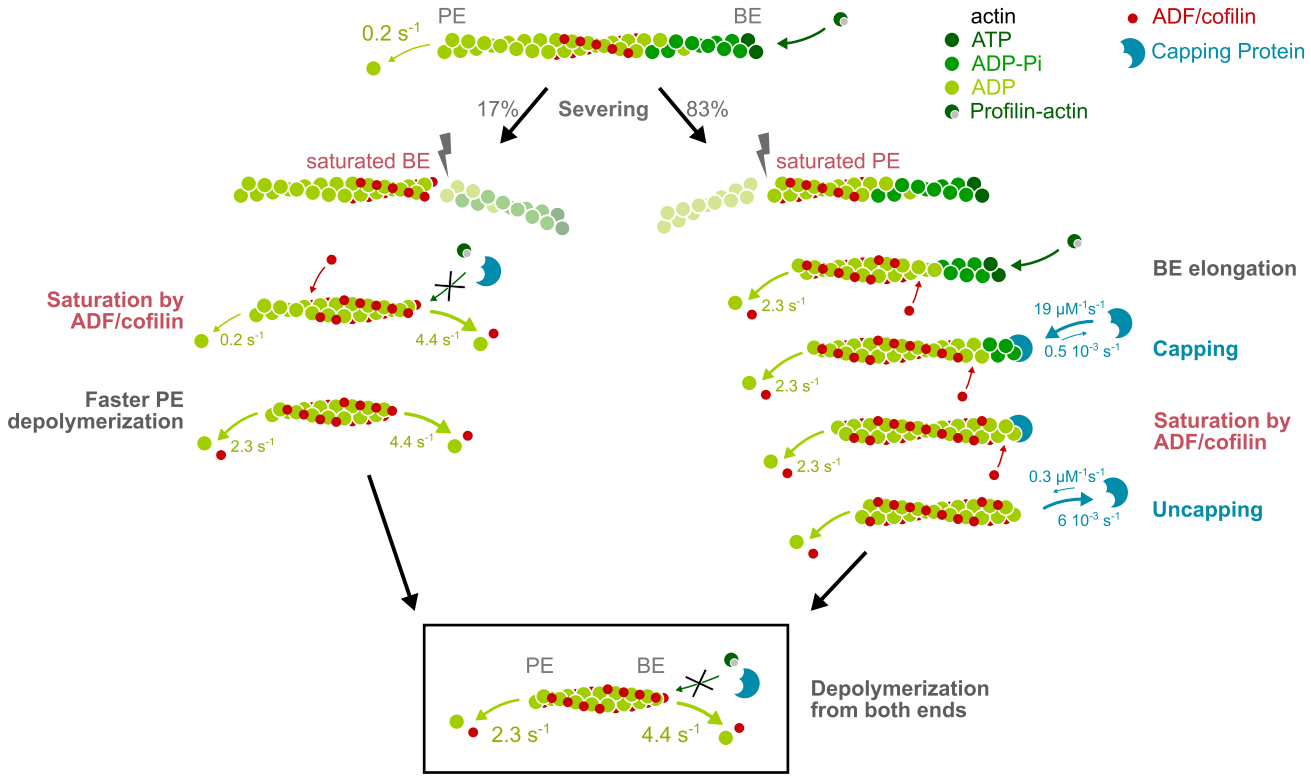

Figure 7. Schematic Summary of ADF/Cofilin-Induced Filament Disassembly in the Presence of Profilin-Actin and CP

Top: an actin filament elongates from its BE and depolymerizes slowly from its PE. ADF/cofilin cannot bind to the ATP/ADP-Pi region at the barbed end, and forms domains on the "older" ADP-actin region of the filament. Severing occurs at domain boundaries, generating a new saturated BE (17% of cases) or a new saturated PE (83%). Middle, left: the newly generated saturated BE starts depolymerizing despite the presence of profilin-actin and CP. The PE depolymerizes slowly and the ADF/cofilin domain grows toward the PE, until the filament is fully decorated. Middle, right: ADF/cofilin accelerates the depolymerization of the new saturated PE while the filament still elongates from its BE, until it is capped by CP. ADF/cofilin can then fully decorate the filament, inducing the uncapping of the BE and its depolymerization. Bottom: ADF/cofilin-saturated filaments do not treadmill but depolymerize from both ends. The indicated depolymerization rates correspond to α-skeletal actin and ADF. Other rates can be found in Figure 4C.

Collectively, our results provide evidence that CP and ADF/cofilin act together to age filaments, turning them into ADF/cofilin-saturated ADP-actin filaments, which depolymerize from both ends (Figure 7).

DISCUSSION

Mechanisms of ADF/Cofilin-Induced Disassembly

Looking at large populations of individual actin filaments in controlled conditions has allowed us to quantify the different reactions underlying filament disassembly by ADF/cofilin: the formation of domains, their growth dynamics, their severing dynamics, and the depolymerization of filaments from both ends. We find that cofilin domains expand equally fast in both directions on ADP-F-actin, and that beyond a minimal domain size severing occurs at a constant rate for each domain.

About 83% of severing events generate filament fragments with ADF/cofilin-saturated pointed ends, which depolymerize faster than bare filament pointed ends. The extent of this effect is isoform dependent, ADF being far more potent than cofilins. These severing events also generate bare barbed ends. Their outcome depends on the proteins present in the cytoplasm. If no ATP-G-actin is present, free ADF/cofilin directly targets these barbed ends and enhances their depolymerization (Figure 3). In cells, such a situation is probably rare. It may be encountered in regions depleted of G-actin, or when nucleotide exchange is slow and ADP-G-actin is the dominant monomer species. In the presence of ATP-G-actin, barbed ends are able to elongate, with a terminal ATP-actin subunit protecting them from the action of ADF/cofilin (Figure 3G), and new growing filaments are thus generated by severing. When CP is also present, these growing barbed ends eventually get capped, allowing the filaments to become fully saturated by ADF/cofilin. The barbed ends then lose their CP and depolymerize (Figure 6), slower than bare barbed ends, again in an ADF/cofilin isoform-dependent manner (Figure 4). Strikingly, this depolymerization can hardly be stopped by CP and ATP-G-actin in solution (Figure 7, right).

The remaining 17% of severing events take place at the boundary of domains toward the barbed-end side, and thus directly generate ADF/cofilin-saturated barbed ends (Figure 7, left). They depolymerize in the unstoppable manner described in the previous paragraph.

Comparison with Existing In Vitro Data

To our knowledge, only two single-filament studies have measured the depolymerization rates of individual filaments in

the presence of ADF/cofilin. Andrianantoandro and Pollard [27] reported a much slower depolymerization for both ends in the presence of ADF, most likely because they worked at lower pH, and possibly also because filaments contained mixed nucleotide states and were not fully saturated with ADF. Nadkarni and Brieher [23] reported relatively high rates for barbed-end depolymerization in the presence of human cofilin. Their measurements are quite dispersed and can be explained by our results, considering that the filaments they observed exhibited a mixture of two effects: the enhanced depolymerization of bare regions due to free cofilin, and the slower depolymerization of cofilin-saturated regions (as in Figure 3A).

Based on bulk solution measurements, a 25-fold acceleration of pointed-end depolymerization was predicted for ADF/cofilin-saturated filaments [11], much higher than our results (Figure 4). Bulk solution assays, which can only monitor the global outcome of several different reactions, are easily misinterpreted. For instance, now that we know that ADF-saturated filament barbed ends have a 600-fold weaker affinity for CP (Figure 5), we understand that using CP to count the number of barbed ends [37] should lead one to underestimate that number and thus the extent of severing. In addition, the contribution of barbed-end depolymerization that we report here could not be anticipated and was not taken into account: one needs to step out of the frame of filament treadmilling in order to describe the mechanism of ADF/cofilin-induced disassembly (Figure 7).

As we have illustrated in Figure S4, the rate constants that we report here account well for existing data, and provide key information to understand the global effects of ADF/cofilin. For instance, we show that the enhanced severing activity of cofilin-2 compared to cofilin-1 [24] results from a combination of factors. Cofilin-2 domains nucleate and grow faster than cofilin-1 domains, especially on cytoplasmic actin filaments (Figure 1). In addition, cofilin-2 domains sever skeletal actin filaments faster than cofilin-1 domains (Figure 2E). The latter result also explains why cofilin-2 leads to faster severing than cofilin-1 when observed at similar decoration levels [24].

We find that ADF is far more efficient than cofilin-1 or cofilin-2 in depolymerizing filaments: an ADF-saturated filament will depolymerize from its two ends 6-fold faster than a cofilin-saturated filament (Figure 4C), and free ADF will depolymerize bare barbed ends faster than free cofilin-1 (Figures 3C and 3D). These results explain why ADF was previously reported to be a more potent global disassembler of F-actin [8, 28] although it is only moderately more efficient than cofilin-1 (and less efficient than cofilin-2) at severing filaments [24].

Recent single-filament studies have often focused on the initial binding events and the observation of very small cofilin domains [29, 34, 38], whereas here we mostly look at cofilin domains that are larger than 100 nm. We have nonetheless monitored the nucleation and growth of smaller domains by measuring the increase in fluorescence intensity due to the binding of the first labeled molecules. We found that this method led to similar results as tracking the border of larger domains (Figure S2D). Overall, our results indicate that domains expand at a constant rate as soon as they contain a few cofilin molecules. However, we cannot determine whether these very small domains also expand symmetrically. A recent atomic force microscopy study of small domains measured that they grow 4-fold faster toward the pointed end [38], and this result may be a size-related feature. In addition, this technique imposes a strong interaction of the probe with the filament, which also needs to interact with the substrate, and these technical details may also alter domain dynamics. The resolution of our experiment does not allow us to decipher the individual binding events leading to these stable cofilin domains, and we thus could not confront the recent report that cofilin binding cooperativity is a long-range effect [29].

Using yeast proteins, Gressin et al. [34] found that a minimal domain size of 23 cofilin proteins is required for severing, and that this minimum size may be an optimum. Our data, using mammalian cofilins, indicate that fragmentation indeed requires a minimal domain size (estimated to be approximately 100 cofilins), but beyond that threshold the severing rate seems independent of domain size or growth rate (Figure 2D).

Physiological Relevance of Barbed-End Dynamics

Observations in cells have sometimes been difficult to reconcile with the widely accepted notion that filaments should undergo a form of treadmilling, and that depolymerization must take place at the pointed end. For example, Miyoshi et al. [39] found that CP turnover in lamellipodia was very fast and controlled by cofilin, which is difficult to explain with severing and pointed-end depolymerization only. The same authors later found that treadmilling alone could not account for these experimental observations, and proposed that "a substantial amount of F-actin might disassemble near the barbed end of the filament" [40]. Similarly, Kueh et al. [41] observed that cytochalasin D blocked the depolymerization of branched filament networks in bacterial comet tails and cell ruffles, which cannot be explained in the framework of treadmilling. These observations later led Brieher to propose that "just maybe, actin filaments in cells depolymerize from their barbed ends" [42]. We show here that ADF/cofilin-saturated filaments do not treadmill, and that they are in a state that promotes barbed-end depolymerization. This result provides a molecular basis that could explain the paradoxical conclusions of Miyoshi et al. and Kueh et al.

We are thus facing a change in paradigm for actin depolymerization in cells and the role of barbed ends. A new scheme can be proposed (Figure 7) where filaments grow until they get capped, thereby allowing their full saturation by ADF/cofilin, which in turn triggers their uncapping and their depolymerization from the barbed end (in addition to the pointed end). CP appears to play a singular role because, in the presence of ADF/cofilin, it transiently caps filament barbed ends to turn them from a steadily growing state into a steadily depolymerizing one. It is also interesting to note that in cells, CP does not distribute uniformly along the actin-rich lamellipodium but is instead concentrated at its distal edge and displays more rapid dynamics than expected from its association with actin filament barbed ends in vitro [43, 44]. Thus, it is intriguing to speculate that filament uncapping by ADF/cofilin, which localize more proximally along the lamellipodium compared to CP [45], may control the dynamics and localization of CP in lamellipodia.

In cells, various additional factors are likely to modulate the relative contributions of barbed and pointed ends to depolymerization as well as the binding and severing activities of ADF/cofilin. For instance, ADF/cofilin domain growth can be biased toward the pointed end by other side-binding proteins such as

tropomyosins [46]. The requirement that ADF/cofilin domains reach a minimal size to sever filaments implies that short filaments, such as the branches in a lamellipodium, are likely to become saturated without severing. Without additional cofactors, disassembly would then be mostly due to debranching [47, 48] and depolymerization from both ends. Other actin-associated proteins, such as Aip1, were reported to enhance severing of ADF/cofilin-saturated filaments [34, 49]. In this context, Aip1 would help to generate shorter ADF/cofilin-decorated fragments that would further depolymerize from both ends. In the presence of Aip1 and other cofactors, actin filaments also appear insensitive to CPs when depolymerizing [34, 41]. Finally, twinfilin, which is composed of two ADF/cofilin-like domains, was reported to act as a barbed-end capper [50] and works in concert with cyclase-associated protein to depolymerize filament ends and complement the severing activity of cofilin [51].

Together, our results show that ADF/cofilin saturation puts actin filaments into a depolymerizing state. In the future, it will be important to elucidate how other proteins that associate with ADF/cofilin and are involved in actin filament disassembly exploit or compensate this property.

STAR★METHODS

Detailed methods are provided in the online version of this paper and include the following:

- KEY RESOURCES TABLE
- CONTACT FOR REAGENT AND RESOURCE SHARING
- METHOD DETAILS
  - Protein expression and purification
  - Protein labeling
  - Buffers
  - Microfluidic setup
  - Microfluidic experiments
  - Acquisition
- QUANTIFICATION AND STATISTICAL ANALYSIS
  - Specific experiments and analysis
  - Statistical method
- DATA AND SOFTWARE AVAILABILITY
  - Simulations of global experiments
  - Simulations of elongating populations

SUPPLEMENTAL INFORMATION

Supplemental Information includes seven figures, three movies, and two data files and can be found with this article online at http://dx.doi.org/10.1016/j.cub.2017.05.048.

AUTHOR CONTRIBUTIONS

B.G. and Y.S. supplied reagents; H.W., S.M., and G.R.-L. collected data; H.W. and G.R.-L. wrote software; H.W., S.M., A.J., and G.R.-L. analyzed data; G.R.-L. wrote the first draft of the manuscript; H.W., P.L., A.J., and G.R.-L. edited the manuscript; H.W. produced the figures; and P.L., A.J., and G.R.-L. supervised the project.

ACKNOWLEDGMENTS

We thank Christophe Le Clainche and Guillaume Charras for their critical reading of an early draft of the manuscript. We thank all members of the Romet/Jégou lab for help with experiments. We acknowledge funding from the Human Frontier Science Program (grant RGY0066 to G.R.-L.), French Agence Nationale de la Recherche (grant Muscactin to G.R.-L.), European Research Council (grant StG-679116 to A.J.), Fondation ARC pour la Recherche sur le Cancer (postdoctoral fellowship to H.W.), Sigrid Juselius Foundation (grant to P.L.), and FY 2015 Researcher Exchange Program between the Japan Society for the Promotion of Science and the Academy of Finland (grant 292706 to Y.S.).

Received: January 18, 2017
Revised: April 4, 2017
Accepted: May 16, 2017
Published: June 15, 2017

REFERENCES

1. Pollard, T.D., and Cooper, J.A. (2009). Actin, a central player in cell shape and movement. Science *326*, 1208–1212.
2. Blanchoin, L., Boujemaa-Paterski, R., Sykes, C., and Plastino, J. (2014). Actin dynamics, architecture, and mechanics in cell motility. Physiol. Rev. *94*, 235–263.
3. Lappalainen, P., and Drubin, D.G. (1997). Cofilin promotes rapid actin filament turnover in vivo. Nature *388*, 78–82.
4. Ydenberg, C.A., Johnston, A., Weinstein, J., Bellavance, D., Jansen, S., and Goode, B.L. (2015). Combinatorial genetic analysis of a network of actin disassembly-promoting factors. Cytoskeleton *72*, 349–361.
5. Bernstein, B.W., and Bamburg, J.R. (2010). ADF/cofilin: a functional node in cell biology. Trends Cell Biol. *20*, 187–195.
6. Kanellos, G., and Frame, M.C. (2016). Cellular functions of the ADF/cofilin family at a glance. J. Cell Sci. *129*, 3211–3218.
7. Yamaguchi, H., and Condeelis, J. (2007). Regulation of the actin cytoskeleton in cancer cell migration and invasion. Biochim. Biophys. Acta *1773*, 642–652.
8. Vartiainen, M.K., Mustonen, T., Mattila, P.K., Ojala, P.J., Thesleff, I., Partanen, J., and Lappalainen, P. (2002). The three mouse actin-depolymerizing factor/cofilins evolved to fulfill cell-type-specific requirements for actin dynamics. Mol. Biol. Cell *13*, 183–194.
9. Kremneva, E., Makkonen, M.H., Skwarek-Maruszewska, A., Gateva, G., Michelot, A., Dominguez, R., and Lappalainen, P. (2014). Cofilin-2 controls actin filament length in muscle sarcomeres. Dev. Cell *31*, 215–226.
10. Maciver, S.K., and Weeds, A.G. (1994). Actophorin preferentially binds monomeric ADP-actin over ATP-bound actin: consequences for cell locomotion. FEBS Lett. *347*, 251–256.
11. Carlier, M.-F., Laurent, V., Santolini, J., Melki, R., Didry, D., Xia, G.X., Hong, Y., Chua, N.H., and Pantaloni, D. (1997). Actin depolymerizing factor (ADF/cofilin) enhances the rate of filament turnover: implication in actin-based motility. J. Cell Biol. *136*, 1307–1322.
12. Blanchoin, L., and Pollard, T.D. (1998). Interaction of actin monomers with *Acanthamoeba* actophorin (ADF/cofilin) and profilin. J. Biol. Chem. *273*, 25106–25111.
13. Suarez, C., Roland, J., Boujemaa-Paterski, R., Kang, H., McCullough, B.R., Reymann, A.C., Guérin, C., Martiel, J.L., De la Cruz, E.M., and Blanchoin, L. (2011). Cofilin tunes the nucleotide state of actin filaments and severs at bare and decorated segment boundaries. Curr. Biol. *21*, 862–868.
14. Hayden, S.M., Miller, P.S., Brauweiler, A., and Bamburg, J.R. (1993). Analysis of the interactions of actin depolymerizing factor with G- and F-actin. Biochemistry *32*, 9994–10004.
15. De La Cruz, E.M. (2005). Cofilin binding to muscle and non-muscle actin filaments: isoform-dependent cooperative interactions. J. Mol. Biol. *346*, 557–564.
16. McCullough, B.R., Grintsevich, E.E., Chen, C.K., Kang, H., Hutchison, A.L., Henn, A., Cao, W., Suarez, C., Martiel, J.L., Blanchoin, L., et al. (2011). Cofilin-linked changes in actin filament flexibility promote severing. Biophys. J. *101*, 151–159.

17. Breitsprecher, D., Koestler, S.A., Chizhov, I., Nemethova, M., Mueller, J., Goode, B.L., Small, J.V., Rottner, K., and Faix, J. (2011). Cofilin cooperates with fascin to disassemble filopodial actin filaments. J. Cell Sci. *124*, 3305–3318.
18. McGough, A., Pope, B., Chiu, W., and Weeds, A. (1997). Cofilin changes the twist of F-actin: implications for actin filament dynamics and cellular function. J. Cell Biol. *138*, 771–781.
19. Prochniewicz, E., Janson, N., Thomas, D.D., and De la Cruz, E.M. (2005). Cofilin increases the torsional flexibility and dynamics of actin filaments. J. Mol. Biol. *353*, 990–1000.
20. McCullough, B.R., Blanchoin, L., Martiel, J.L., and De la Cruz, E.M. (2008). Cofilin increases the bending flexibility of actin filaments: implications for severing and cell mechanics. J. Mol. Biol. *381*, 550–558.
21. Galkin, V.E., Orlova, A., Kudryashov, D.S., Solodukhin, A., Reisler, E., Schröder, G.F., and Egelman, E.H. (2011). Remodeling of actin filaments by ADF/cofilin proteins. Proc. Natl. Acad. Sci. USA *108*, 20568–20572.
22. De La Cruz, E.M. (2009). How cofilin severs an actin filament. Biophys. Rev. *1*, 51–59.
23. Nadkarni, A.V., and Brieher, W.M. (2014). Aip1 destabilizes cofilin-saturated actin filaments by severing and accelerating monomer dissociation from ends. Curr. Biol. *24*, 2749–2757.
24. Chin, S.M., Jansen, S., and Goode, B.L. (2016). TIRF microscopy analysis of human Cof1, Cof2, and ADF effects on actin filament severing and turnover. J. Mol. Biol. *428*, 1604–1616.
25. Bugyi, B., and Carlier, M.-F. (2010). Control of actin filament treadmilling in cell motility. Annu. Rev. Biophys. *39*, 449–470.
26. Pollard, T.D. (2016). What we know and do not know about actin. In Handbook of Experimental Pharmacology, B.M. Jockusch, ed. (Springer International), pp. 331–347.
27. Andrianantoandro, E., and Pollard, T.D. (2006). Mechanism of actin filament turnover by severing and nucleation at different concentrations of ADF/cofilin. Mol. Cell *24*, 13–23.
28. Yeoh, S., Pope, B., Mannherz, H.G., and Weeds, A. (2002). Determining the differences in actin binding by human ADF and cofilin. J. Mol. Biol. *315*, 911–925.
29. Hayakawa, K., Sakakibara, S., Sokabe, M., and Tatsumi, H. (2014). Single-molecule imaging and kinetic analysis of cooperative cofilin-actin filament interactions. Proc. Natl. Acad. Sci. USA *111*, 9810–9815.
30. Jégou, A., Niedermayer, T., Orbán, J., Didry, D., Lipowsky, R., Carlier, M.F., and Romet-Lemonne, G. (2011). Individual actin filaments in a microfluidic flow reveal the mechanism of ATP hydrolysis and give insight into the properties of profilin. PLoS Biol. *9*, e1001161.
31. Jégou, A., Carlier, M.-F., and Romet-Lemonne, G. (2013). Formin mDia1 senses and generates mechanical forces on actin filaments. Nat. Commun. *4*, 1883.
32. Hayakawa, K., Tatsumi, H., and Sokabe, M. (2011). Actin filaments function as a tension sensor by tension-dependent binding of cofilin to the filament. J. Cell Biol. *195*, 721–727.
33. Niedermayer, T., Jégou, A., Chièze, L., Guichard, B., Helfer, E., Romet-Lemonne, G., Carlier, M.-F., and Lipowsky, R. (2012). Intermittent depolymerization of actin filaments is caused by photo-induced dimerization of actin protomers. Proc. Natl. Acad. Sci. USA *109*, 10769–10774.
34. Gressin, L., Guillotin, A., Guérin, C., Blanchoin, L., and Michelot, A. (2015). Architecture dependence of actin filament network disassembly. Curr. Biol. *25*, 1437–1447.
35. Lappalainen, P., Fedorov, E.V., Fedorov, A.A., Almo, S.C., and Drubin, D.G. (1997). Essential functions and actin-binding surfaces of yeast cofilin revealed by systematic mutagenesis. EMBO J. *16*, 5520–5530.
36. Hild, G., Kalmár, L., Kardos, R., Nyitrai, M., and Bugyi, B. (2014). The other side of the coin: functional and structural versatility of ADF/cofilins. Eur. J. Cell Biol. *93*, 238–251.
37. Didry, D., Carlier, M.F., and Pantaloni, D. (1998). Synergy between actin depolymerizing factor/cofilin and profilin in increasing actin filament turnover. J. Biol. Chem. *273*, 25602–25611.
38. Ngo, K.X., Kodera, N., Katayama, E., Ando, T., and Uyeda, T.Q. (2015). Cofilin-induced unidirectional cooperative conformational changes in actin filaments revealed by high-speed atomic force microscopy. eLife *4*, 1–22.
39. Miyoshi, T., Tsuji, T., Higashida, C., Hertzog, M., Fujita, A., Narumiya, S., Scita, G., and Watanabe, N. (2006). Actin turnover-dependent fast dissociation of capping protein in the dendritic nucleation actin network: evidence of frequent filament severing. J. Cell Biol. *175*, 947–955.
40. Miyoshi, T., and Watanabe, N. (2013). Can filament treadmilling alone account for the F-actin turnover in lamellipodia? Cytoskeleton *70*, 179–190.
41. Kueh, H.Y., Charras, G.T., Mitchison, T.J., and Brieher, W.M. (2008). Actin disassembly by cofilin, coronin, and Aip1 occurs in bursts and is inhibited by barbed-end cappers. J. Cell Biol. *182*, 341–353.
42. Brieher, W. (2013). Mechanisms of actin disassembly. Mol. Biol. Cell *24*, 2299–2302.
43. Mejillano, M.R., Kojima, S., Applewhite, D.A., Gertler, F.B., Svitkina, T.M., and Borisy, G.G. (2004). Lamellipodial versus filopodial mode of the actin nanomachinery: pivotal role of the filament barbed end. Cell *118*, 363–373.
44. Lai, F.P., Szczodrak, M., Block, J., Faix, J., Breitsprecher, D., Mannherz, H.G., Stradal, T.E., Dunn, G.A., Small, J.V., and Rottner, K. (2008). Arp2/3 complex interactions and actin network turnover in lamellipodia. EMBO J. *27*, 982–992.
45. Svitkina, T.M., and Borisy, G.G. (1999). Arp2/3 complex and actin depolymerizing factor/cofilin in dendritic organization and treadmilling of actin filament array in lamellipodia. J. Cell Biol. *145*, 1009–1026.
46. Gateva, G., Kremneva, E., Reindl, T., Kotila, T., Kogan, K., Gressin, L., Gunning, P.W., Manstein, D.J., Michelot, A., and Lappalainen, P. (2017). Tropomyosin isoforms specify functionally distinct actin filament populations in vitro. Curr. Biol. *27*, 705–713.
47. Blanchoin, L., Pollard, T.D., and Mullins, R.D. (2000). Interactions of ADF/cofilin, Arp2/3 complex, capping protein and profilin in remodeling of branched actin filament networks. Curr. Biol. *10*, 1273–1282.
48. Chan, C., Beltzner, C.C., and Pollard, T.D. (2009). Cofilin dissociates Arp2/3 complex and branches from actin filaments. Curr. Biol. *19*, 537–545.
49. Jansen, S., Collins, A., Chin, S.M., Ydenberg, C.A., Gelles, J., and Goode, B.L. (2015). Single-molecule imaging of a three-component ordered actin disassembly mechanism. Nat. Commun. *6*, 7202.
50. Helfer, E., Nevalainen, E.M., Naumanen, P., Romero, S., Didry, D., Pantaloni, D., Lappalainen, P., and Carlier, M.-F. (2006). Mammalian twinfilin sequesters ADP-G-actin and caps filament barbed ends: implications in motility. EMBO J. *25*, 1184–1195.
51. Johnston, A.B., Collins, A., and Goode, B.L. (2015). High-speed depolymerization at actin filament ends jointly catalysed by twinfilin and Srv2/CAP. Nat. Cell Biol. *17*, 1504–1511.
52. Spudich, J.A., and Watt, S. (1971). The regulation of rabbit skeletal muscle contraction. I. Biochemical studies of the interaction of the tropomyosin-troponin complex with actin and the proteolytic fragments of myosin. J. Biol. Chem. *246*, 4866–4871.
53. Schuler, H., Karlsson, R., and Lindberg, U. (2006). Purification of Non-muscle Actin, Third Edition (Elsevier).
54. Casella, J.F., Maack, D.J., and Lin, S. (1986). Purification and initial characterization of a protein from skeletal muscle that caps the barbed ends of actin filaments. J. Biol. Chem. *261*, 10915–10921.
55. Gieselmann, R., Kwiatkowski, D.J., Janmey, P.A., and Witke, W. (1995). Distinct biochemical characteristics of the two human profilin isoforms. Eur. J. Biochem. *229*, 621–628.
56. Cao, W., Goodarzi, J.P., and De La Cruz, E.M. (2006). Energetics and kinetics of cooperative cofilin-actin filament interactions. J. Mol. Biol. *361*, 257–267.
57. Kaplan, E.L., and Meier, P. (1958). Nonparametric estimation from incomplete observations. J. Am. Stat. Assoc. *53*, 457–481.
58. Gillespie, D.T. (1977). Exact stochastic simulation of coupled chemical reactions. J. Phys. Chem. *81*, 2340–2361.

STAR★METHODS

KEY RESOURCES TABLE

REAGENT or RESOURCE	SOURCE	IDENTIFIER
Bacterial and Virus Strains		
BL21(DE3)	Thermo Fischer	Cat# C600003
BL21 (DE3) Star	Thermo Fischer	Cat# C601003
Biological Samples		
Rabbit muscle acetone powder	Pel-freeze	Cat#41995-2
Bovine spleen	Vainio Slaughterhouse, Orimattila, Finland	N/A
Human erythrocytes	Etablissement Francais du Sang	N/A
Chemicals, Peptides, and Recombinant Proteins		
Alexa488- succimidyl ester	Life Technologies	Cat#A20000
Alexa594- succimidyl ester	Life Technologies	Cat#A20004
EZ-Link Sulfo-NHS-Biotin	Thermo Scientific	Cat#21338
Critical Commercial Assays		
AKTA Pure system	GE Healthcare	N/A
Recombinant DNA		
Mouse cofilin-1, mCherry-cofilin-1, eGFP-cofilin-1	[9]	Uniprot: P18760
Mouse cofilin-2, mCherry-cofilin-2, eGFP-cofilin-2	[9]	Uniprot: P45591
K96A D98A cofilin-1	This paper	N/A
Human ADF	Lab of M.F. Carlier	Uniprot: P60981
Human Profilin I	Lab of M.F. Carlier	Uniprot: P07737
Mouse Capping Protein alpha1	Lab of M.F. Carlier	Uniprot: P47753
Mouse Capping Protein beta2	Lab of M.F. Carlier	Uniprot: P47757
Human gelsolin	Lab of M.F. Carlier	Uniprot: P06396
Software and Algorithms		
Simulation of global severing and depolymerizing experiments	This paper	Data S1
Simulation of the outcome of an elongating filament population	This paper	Data S2
Other		
HiTrap Q FF column	GE Healthcare	Cat#17-5156-01
Hitrap SP column	GE Healthcare	Cat#17-5157-01
HisTrap FF Crude affinity column	GE Healthcare	Cat#17-5248-02
HiLoad 16/60 Superdex 200 gel filtration column	GE Healthcare	Cat#28-9893-35
Protino Ni-NTA Agarose beads	Macherey-Nagel	Cat#745400.25
Glutathione Sepharose beads	GE Healthcare	Cat#17-0756-01

CONTACT FOR REAGENT AND RESOURCE SHARING

Further information and requests for resources and reagents should be directed to and will be fulfilled by the Lead Contact, Guillaume Romet-Lemonne (romet@ijm.fr).

METHOD DETAILS

Protein expression and purification

Skeletal muscle actin was purified from rabbit muscle acetone powder (Pel-freeze) following the standard protocol of Spudich and Watt [52]. The powder was resuspended in X-buffer (2 mM Tris pH 7.8, 0.5 mM ATP, 0.1mM CaCl2, 1mM DTT and 0.01% NaN3) and centrifuged at 4,000 g, keeping the supernatant which was then filtered through cheese cloth. To remove contaminants, 3.3M KCl was added and the solution was centrifuged at 4,000 g, keeping the supernatant, which was again filtered through cheese cloth. The solution was dialysed overnight in 1mM MgCl2 and 100mM KCl to polymerize filaments, followed by the addition of 800mM KCl

to dissociate contaminating proteins from the filaments. After centrifugation at 100,000 g, the pellet was resuspended and dialyzed in G-buffer to depolymerize. Aggregates were removed from the solution by centrifugation at 100,000 g. Remaining contaminants were eliminated by gel filtration in a Superdex 200 HiLoad column (GE Healthcare). G-actin was stored in G-buffer (2 mM Tris pH 7.8, 0.2 mM ATP, 0.1 mM CaCl2, 1 mM DTT and 0.01% NaN3), on ice, for up to 8 weeks.

Cytoplasmic actin was purified from bovine spleen adapting the procedure detailed in Schuler et al. [53]. Specifically, fresh bovine spleen was homogenized and the profilin-actin complex was extracted using a poly-L-proline column. Actin was separated from profilin by polymerization-depolymerization cycles and both proteins were stored at −80°C until further use.

Spectrin-actin seeds were purified from human erythrocytes as described in Casella et al. [54]. Ghosts were prepared from human erythrocytes, which were first washed by repeated cycle of centrifugation (3000 g at 4°C for 15min) and pellet resuspension in PBS buffer with EDTA (5 mM NaPO4 pH 7.7, 150 mM NaCl, 1 mM EDTA). Erythrocytes were lysed in low ionic strength buffer (5 mM NaPO4 pH 7.7, 1 mM PMSF) to turn them into ghosts. Ghosts were then washed and concentrated by 3 cycles of centrifugation (45,000 g at 4°C for 15min) and pellet resuspension in Washing buffer (5 mM NaPO4 pH 7.7, 0.1 mM PMSF). The final ghost pellet was then incubated at 37°C for 40 min with occasional mixing, and then centrifuged at 400,000 g at 4°C for 1 hr ro remove membrane residues. The supernatant was complemented with 2 mM DTT and protease inhibitors, and an equal volume of ice-cold glycerol was added. Concentration was determined by adding actin-pyrene and measuring the number of growing filament ends, using a spectrometer to measure the amount of F-actin-pyrene over time. Aliquots of the spectrin-actin seed solution were stored at −20°C until used.

Recombinant human profilin I (Uniprot: P07737) was expressed in E. Coli and purified following the protocol described by Gieselmann et al. [55]. Profilin I was expressed in *E. coli* using the bacteriophage T7 expression system, and the plasmid was transformed into strain BL21 DE3 Star (Thermo Fischer). Protein expression was induced with 1 mM IPTG, 2.5 hr at 37°C. After centrifugation at 2,000 g the pellet was resuspended in Lysis buffer (Tris 50 mM pH 7.3, 5 mM EGTA, 0.1 mM EDTA, 50 mM KCl, 10 mM DTT, 8 M urea, 0.1% Tween-20, 1 mM PMSF, inhibitors). After sonication, the lysate was centrifuged at 4°C for 30 min at 186,000 g and the supernatant was dialysed overnight at 4°C against Dialysis buffer (Tris 50 mM pH 7.3, 1 mM EGTA, 0.1 mM EDTA, 50 mM KCl, 1 mM DTT). The protein solution was loaded onto a poly-L-proline column, washed with 3 column volumes of Washing buffer (mixture of 3 volumes of Dialysis buffer + 1 volume Elution buffer), and eluted with Elution buffer (Tris 50 mM pH 7.3, 5 mM EGTA, 0.1 mM EDTA, 50 mM KCl, 10 mM DTT, 8 M urea). Peak fractions were pooled, dialysed overnight at 4°C against Dialysis buffer, concentrated with Vivaspin 10kDa, and dialysed overnight at 4°C against Conservation buffer (Tris 10 mM pH 7.5, 50 mM KCl, 1 mM DTT). The concentration was determined by absorbance at 280 nm using the calculated extinction coefficient (17,020 $M^{-1}cm^{-1}$). The protein solution was aliquoted, flash-frozen and stored a −80°C.

Mouse cofilin-1 (Uniprot: P18760) and cofilin-2 (Uniprot: P45591), as well as fluorescently tagged cofilins (see next subsection, ''protein labeling'') were purified as described previously in Kremneva et al. [9]. In detail, Mouse cofilin-1 and cofilin-2 were expressed in E.coli as glutathioneS-transferase (GST) fusion proteins. GST fusion proteins were enriched from the lysis supernatant with glutathione Sepharose beads (GE Healthcare). ADF/cofilins were cleaved off the GST with 1U of Prescission protease (GE Healthcare) for 100μg of protein, and further purified by a Superdex-200 HiLoad gel filtration column (GE Healthcare). The peak fractions that eluted from the column at 83 mL were pooled and concentrated with a Vivaspin 10kDa to ∼500 μM.

PCR based mutagenesis was performed to generate the K96A D98A mutant of cofilin-1. The primers were as follows (lowercase letters indicate the mutations): 5′ GGAGAGCAAGgcGGAGGcCCTGGTGTTCATC 3′ (forward) and 5′ GATGAACACCAGGg CCTCCgcCTTGCTCTCC 3′ (reverse).

Human ADF (hADF, Uniprot: P60981) were produced using BL21 DE3 Star E. Coli. One liter of LB media supplemented with 100 μg/mL ampicillin was grown at 200 rpm and at 37°C until the A600 was between 0.6 and 0.8. hADF were produced by supplementing the media with 1 mM of IPTG and by growth for 2.5 hr at 37°C, 200 rpm. Cells were harvested by centrifugation (2,000 g for 15 min, at 4°C), washed once in ice cold 100 mL of 10 mM Tris HCl pH 7.5, 1 mM EDTA, then resuspended into 100mL of 10 mM Tris HCl pH 7.5, 1 mM EDTA, 1% triton, 5% glycerol, and CLAP inhibitors. After 20 min of mild agitation at 4°C, 50 mg of lysozyme were added. Cells were further incubated for 30 min at 4°C. Media was then supplemented with 1 mg of DNase I and 5 mM of MgCl2, and were incubated for another 30 min at 4°C under mild agitation. 0.1 mM PMSF was added prior to sonication (for a total duration of 5 min, alternating between 1 s on, 1 s off). Lysate was pelleted at 100,000 g for 30 min, at 4°C. The supernatant was loaded on a HiTrap Q column equilibrated with 10 mM Tris HCl pH 7.5, 0.2 mM EGTA, 50 mM NaCl, 0.1% NaN3. The flow through was collected and concentrated using a vivaspin 10 kDa down to a volum of 10 mL. The sample was dialysed overnight against 1 l of 10 mM Pipes pH 6.5, 25 mM NaCl, 5 mM DTT, 0.1mM EGTA, 0.01% NaN3, then loaded onto a HiTrap SP column equilibrated with the same buffer. The elution is achieved by applying a gradient up to 1 M NaCl. Fractions of the relevant peak were pooled, concentrated and dialysed overnight at 4°C against 1 L of 5 mM Tris HCl pH 7.5, 1 mM DTT, 0.01% NaN3. The sample was centrifugated for 15 min at 430,000 g before measuring hADF concentration (ε280 = 10,300 M-1.cm-1), and flashed frozen in liquid nitrogen for long term storage at −80°C.

The plasmid for the expression of mouse capping protein α1 (Uniprot: P47753) and β2 (Uniprot: P47757) subunits was constructed in a pRSFDuet-1 vector, providing a 6xHis tag at the N terminus of the α1 subunit. Mouse capping protein α1β2 was expressed and purified from BL21(DE3) *Escherichia coli*. One liter of LB media containing 50 μg/mL kanamycin was grown shaking at 200 rpm at 37°C until the A600 nm was between 0.6 and 0.8. Expression was induced by the addition of 1mM of IPTG and by growth overnight at 16°C. Cells were harvested by centrifugation (2,000 g for 15 min, at 4°C), washed once in ice cold 30 mL of PBS. Cells were resuspended into 20mM NaPO4 pH 7.8, 500 mM NaCl, 1 mM DTT, 0.1 mM EDTA, 0.1 mM PMSF, CLAP inhibitors, 0.5% Tween and 15 mM imidazole. After 20 min of mild agitation at 4°C, ∼10 mg of lysozyme were added. Cells were further incubated for 20 min. Cells

were sonicated for a total duration of 8 min with 1 s on, 1 s of rest. Lysate is pelleted at 150,000 g for 20 min. Supernatant lysate was purified using a 5 mL HisTrap FF Crude affinity column on a AKTA Pure system (GE Healthcare Life sciences), using an imidazole gradient, up to 500 mM. Fractions from the second peak were pooled and dialysed (membrane cutoff 12,000 kDa) overnight against 2 L of 20 mM Tris-HCl pH 7.5, 50 mM KCl, 1 mM DTT. The sample was centrifugated for 10 min at 7,000 g, concentrated using vivaspin (cutoff 30 kDa) down to 1 mL and injected onto HiLoad 16/60 Superdex 200 gel filtration column. Relevant fractions were pooled, the protein of mouse capping protein $\alpha 1\beta 2$ were measured using an exctinction coefficient at 280nm of 79,540 M-1.cm-1, and flash frozen using liquid nitrogen for $-80°C$ long term storage.

Recombinant human gelsolin (Uniprot: P06396) was produced using BL21 DE3 Star E. Coli. One liter of LB media supplemented with 100 μg/mL ampicillin was grown at 200 rpm and at 37°C until the A600 was between 0.6 and 0.8. Gelsolin proteins were produced by supplementing the media with 1 mM of IPTG and by growth for 4 hr at 37°C, 200 rpm. Cells were harvested by centrifugation (2,000 g for 15 min, at 4°C), washed once in ice cold 100 mL of PBS, then resuspended into 100mL of 50 mM Tris HCl pH 7.8, 1 mM EDTA, 100 mM NaCl, 1 mM PMSF and CLAP inhibitors. After 30 min of mild agitation at 4°C, 10 mg of lysozyme were added. Cells were further incubated for 5 min at 4°C. Media was then supplemented with 2.5 mM EDTA, 1 mg of DNaseI and 5 mM of MgCl2, and were incubated for another 10 min at 4°C under mild agitation. Sonication (for a total duration of 5 min, alternating between 1 s on, 1 s off). Lysate was pelleted at 100,000 g for 30 min, at 4°C. The supernatant was loaded on a HiTrap Q column equilibrated with 20 mM Tris HCl pH 7.8, 1 mM EGTA, 0.01% NaN3. A gradient up to 500mM NaCl was done and fractions from the peak corresponding to the middle of the gradient were pooled before being dialysed overnight against 10 mM MES pH 6.5, 1 mM EGTA, 0.01% NaN3.

The sample was injected onto an equilibrated HiTrap S column and a gradient elution was performed up to 1 M NaCl. The last peak contained the gelsolin proteins in high purity. Proteins were dialysed overnight at 4°C against 2 L of 20 mM Tris HCl pH 7.5, 150 mM NaCl, 0.01% NaN3. Gelsolin concentration was measured using $\varepsilon 280 = 115{,}000\ M^{-1}.cm^{-1}$ before being flash frozen for $-80°C$ long term storage.

Gelsolin were further biotinylated with sulfo-NHS-biotin (EZ-Link Sulfo-NHS-Biotin Reagents, spacer arm length 1.35 nm; Thermo Scientific) following standard procedure.

Protein labeling

Actin was fluorescently labeled on accessible surface lysines of F-actin, using Alexa 488 or Alexa-594 succimidyl ester (Life Technologies). To minimize potential effects from the fluorophore we used a labeling fraction of 15% in our experiments. Apart from photo-induced dimers which cause pauses during depolymerization [33], assembly kinetics were unaffected by the fluorophore [30].

Cofilin-1 and -2 were labeled with mCherry or eGFP at their N terminus [9]. In detail, the fluorescently tagged proteins were cloned in pHAT vector yielding plasmids pPL 687 or pPL 688. Both plasmids contain N-terminal 6xHis tag and a 6 amino acid linker region (SGLRSG) between mCherry/GFP and cofilin. Fluorescent cofilins were expressed and purified with Protino Ni-NTA Agarose beads (Macherey-Nagel) in a buffer containing 20 mM Tris pH 7.5, 250 mM NaCl, 5 mM Imidazole, 0.2 mM phenylmethylsulfonyl fluoride (PMSF). Beads were washed with buffer 20 mM Tris pH 7.5, 250 mM NaCl, 5 mM Imidazole and in elution the concentration of imidazole was increased to 300 mM. Proteins were further purified with Superdex 200 gel filtration column in buffer 10 mM Tris pH 7.5, 150 mM NaCl. Purified proteins were concentrated to volume of 2-3 mL. Concentrations of these proteins were determined by absorbance at 280 nm using their calculated extinction coefficients.

Except when specified otherwise, we used 100% labeled cofilins for binding and severing measurements (Figures 1 and 2), and unlabeled ADF/cofilin for filament depolymerization (Figures 3, 4, 5, and 6).

Buffers

We performed most experiments in F-buffer: 5 mM Tris-HCl pH 7.8, 50 mM KCl, 1 mM MgCl2, 0.2 mM EGTA, 0.2 mM ATP, 10 mM DTT and 1 mM DABCO. DTT and DABCO limit light-induced artifacts. In some experiments measuring bare filament depolymerization (Figures 3C–3F), KCl concentration was raised to 100 mM to slow down the side-binding of ADF/cofilin and thus be able to measure bare BE depolymerization over a larger range of ADF/cofilin concentrations. To measure ADP-Pi-actin depolymerization rates, we used a phosphate buffer with a 17mM Pi concentration, keeping the same ionic strength and similar pH as in our experiments on ADP-actin. This buffer had the same composition as F-buffer, where Tris was replaced with 27.7 mM K_2HPO_4, 17.3 mM KH_2PO_4 (pH 7.0), and there was no KCl.

Microfluidic setup

Protein solutions were injected into a Poly Dimethyl Siloxane (PDMS, Sylgard) chamber, 20 μm in height, $\sim$800 μm in width and $\sim$1 cm in length. Chambers were mounted on glass coverslips previously cleaned in ultrasound baths of 1M NaOH, ethanol and dH_20. PDMS chambers and glass coverslips were UV-treated to allow them to bind tighly to each other. We used cross-shaped channels with 3 or 4 inlets (Figure 1A). We controled the pressure in the reservoir and measured the flow rate in each channel using an MFCS and Flow Units (Fluigent).

Microfluidic experiments

The chamber was first filled with F-buffer without KCl. We then injected actin-spectrin seeds, 10 pM for $\sim$5 min, which adsorbed to the glass surface non-specifically. The surface was then passivated with bovine serum albumin (BSA, 5%) for at least 10 min.

Filament elongation and aging

Filaments were elongated from a solution of 0.8 to 1 μM ATP-G-actin supplemented with an equimolar concentration of profilin to prevent filament nucleation in solution. Filaments were then aged with a second ATP-G-actin solution at the critical concentration of 0.1 μM for 15 min, after which time more than 99% of the monomers were in the ADP state [30]. We made sure filaments did not grow significantly during this aging phase.

Unlabeled filaments

In order to avoid any effect of fluorophores, we used unlabeled actin as often as possible (see binding and severing measurements, Figures 1 and 2). To locate filaments we grew labeled segments, before and after elongating with unlabeled actin, thereby generating labeled regions at the PE and BE ends (Figures 1D and 2C).

PE dynamics

To study depolymerization at the PE, we use gelsolin, an actin binding protein which caps barbed ends. The surface was first passivated with 0.1% biotin-BSA for 10 min and 5% BSA for 10 min. We then injected 3 μg/mL neutravidin for 5 min, followed by 5 pM biotin-gelsolin for ~5 min. The resulting gelsolin-coated surface was kept in F-buffer supplemented with 0.4 mM $CaCl_2$.

Actin filaments were generated in solution using a 4 μM ATP-G-actin solution left to polymerize for at least 2 hr in F-buffer. Before injection into the microfluidic chamber, actin was diluted to 2 μM into F-buffer supplemented with 0.4 mM $CaCl_2$ to allow gelsolin binding.

Control experiments

We varied the flow rate of the incoming solutions, and found that it had no impact on our measurements (Figure S1A).

We verified that actin labeling had no impact on our results (Figures S1B and S1C). Measurements that required the direct visualization of cofilin-1 and cofilin-2 were repeated with different labeling fractions to ensure that labeling had no impact on the results (Figure S1D). Other measurements in this article were systematically carried out with unlabeled ADF/cofilin. We nonetheless repeated these measurements with labeled cofilin-1 and cofilin-2 in order to assess the impact of labeling (Figures S1E and S1F).

All experiments were performed at room temperature.

Acquisition

The microfluidic setup was placed on a Nikon TiE or TE2000 inverted microscope, equiped with a 60x oil-immersion objective and an optional additional 1.5x magnification. We either used TIRF, HiLo or epifluorescence depending on the background fluorophore concentration in solution. The TiE microscope was controlled by Metamorph, illuminated in TIRF or epifluoresence by 100mW tunable lasers (ILAS2, Roper Scientific), and images were acquired by an Evolve EMCCD camera (Photometrics). The TE2000 microscope was controlled by micromanager, illuminated with a 120W Xcite lamp (Lumen dynamics) and images were acquired by an sCMOS Orca-Flash2.8 camera (Hamamatsu).

QUANTIFICATION AND STATISTICAL ANALYSIS

Specific experiments and analysis

Experiments were analyzed either manually on ImageJ for measurements and Microsoft Office Excel for statistical analysis, or automatically using Python algorithms.

Python automated filament tracking

In order to facilitate and improve the accuracy of our measurements, we wrote an algorithm in Python which can automatically track filament elongation and depolymerization as well as the boundaries of cofilin domains (Figures 1F and 1G). Typical packages were used, such as numpy for basic math, skimage for image processing, and scipy for image convolution and data fitting.

The algorithm works as follow: the user first indicates an empty region to get the background intensity, and a typical isolated filaments to estimate the fluorescence of labeled actin or cofilin. Each image is then convoluted with a mask to detect horizontal lines (i.e., filaments) and different thresholds (fluorescence, size, etc) are applied to isolate filaments and cofilin domains on each frame. The algorithm finally extracts the length/size over time of objects and the user can manually delete those with unwanted behaviors (e.g., light-induced pauses during depolymerization, fragmentation, cofilin domains reaching filament ends, false positives). Results are finally fitted with numpy *polyfit* or scipy *curve_fit* functions.

Cofilin domain appearance

We isolated segments of unlabeled actin of fixed length l and searched for the first eGFP-cofilin-1 or eGFP-cofilin-2 to appear on each segment, excluding the regions close to the filament ends (we measured the cofilin fluorescence over time on ImageJ, to determine the frame at which the domain was created). We then calculated the survival fraction of segments without any domain (Figure S2A) which was fitted with a simple exponential in Excel,

$$f_{surv} = exp(-t.l.k_{on,domain}),$$

where l is the segment length in actin monomers, and $k_{on,domain}$ is the effective domain appearance rate.

Domain growth rate

Given that cofilin domains appear quickly but grow slowly on skeletal actin compared to cytoplasmic actin (Figures 1E and 1G), it is difficult to observe individual domains growing for several pixels on skeletal actin filaments. We then implemented two different methods to estimates the growth rate, following the total intensity (used on skeletal actin) and tracking domain edges (cytoplasmic actin).

Measuring domain intensity (Figure S2C)

On ImageJ, the total fluorescence of a 6 by 3 to 4 pixel region was followed over time and fitted on Excel with a linear function, from its appearance until severing or merging with neighboring domains. To estimate the fluorescence of a single eGFP-cofilin, we measured that of a fully saturated actin segment, and divided that value by the number of binding site (i.e., actin monomers).

This approach worked well on small domains (up to 4 pixels, ~400 monomers) but it does not provide independent measurements for growth toward the BE and toward the PE.

Tracking domain borders

We used the automated Python algorithm to track the domain borders. Yet, to reduce the amount of false positives, the user first selects unlabeled filaments on ImageJ and uploads their coordinates onto Python. The cofilin intensity profile is then calculated along each filament and domain borders position are fitted with subpixel resolution based on a threshold value of 40% of the maximum fluorescence (i.e., when eGFP-cofilin saturates filaments). The user then selects the relevant borders tracks (single domains, far from filament ends) which are then fitted with a linear function yielding the growth rate toward the PE or toward the BE. The overall domain growth rate is finally calculated by adding the growth rates toward both ends.

From domain growth rates to cofilin binding constants

Given the growth rate of domains for different cofilin concentrations, one can estimate the binding dynamics at domain edges. We assume the simplest linear model where ADF/cofilin binds the nearest empty position along the filament with equal rates toward the PE and BE. With our limited experimental resolution, it is not possible to tell at which distance to the domain individual cofilin monomers bind. The overall domain growth rate is fitted on Excel with a linear function,

$$v_{growth} = 2.\left(k_{on,edge}.C_{cof} - k_{off,edge}\right)$$

where C_{cof} is the eGFP-cofilin concentration in solution, $k_{on,edge}$ the binding rate at domain borders and $k_{off,edge}$ the unbinding rate. The binding and unbinding rate are estimated per domain border (hence the factor 2).

Unbinding from within domains

To measure the off-rate of ADF/cofilin inside domains we performed a chase experiment in which a labeled filament was saturated with 1 μM of unlabeled ADF or cofilin-1 for 2 min before switching to a solution of 1 μM mCherry-cofilin-1. At such a concentration, the binding at domain edges is of the order of 10 s^{-1}, is much faster than the off-rate, $k_{off,border} \simeq 0.5\ s^{-1}$. We assume that mCherry-coflin-1 binds any empty spot before a gap in the domain forms. Any mCherry-coflin-1 binding thus corresponds to the unbinding of an unlabeled ADF/cofilin inside a domain.

We compared the mean mCherry-cofilin-1 fluorescence over several filaments over time, normalized by that of a fully saturated filament in control experiments (without pre-saturation with unlabeled ADF/cofilin). We observed that a faint and homogeneous mCherry-coflin-1 signal appeared on the timescale of tens of minutes (Figure 1I). The fluorescent signal was fitted on Excel with a linear function (local approximation of an exponential). We excluded the first two data points because the initial rapid increase in signal might mostly be due to an increase in the background noise, including binding to the surface (adding these 2 points to the fit would increase the rate $k_{off,inside}$ by a factor two).

Severing location

To determine where severing occurs, we generated small and sparse mCherry-coflin-1 domains onto Alexa 488-actin filaments. 1 to 2 μM mCherry-coflin-1 was injected for 2 to 5 s before switching to F-buffer only to observe severing (Figure 2A). The vast majority of these events (> 90%) occur at domain borders. Among such events, we then quantified how many would leave generate a bare BE (and coflin-1-saturated PE) versus bare PE (and coflin-1-saturated BE, Figure 2B).

Severing rate

To avoid any effect of the Alexa fluorophore, we measured the severing rate on unlabeled actin filament. Yet in such a case, one cannot tell exactly where severing event occur. Given that we found ~80% of severing to happen at domain borders toward the PE, we assume that whenever domain disappear, it is due to the domain closest to the PE (all filaments where grown from spectrin seeds).

Experiments were performed as follow: actin filaments were grown with a large unlabeled hydrolyzed segment. eGFP-coflin-1 or eGFP-coflin-2 was then injected at low concentration such that few small domains would appear (Figure 2C). We then manually identified on ImageJ all domains on the unlabeled actin segment and determined the frame on which they appeared based on the fluorescence signal. We then calculated the survival fraction (Figure S2A): given a set of domains appearing at time 0, how many have not severed by time t? We accounted for lost domains that may have not severed but could not be further observed (e.g., domain 1 on Figure 2C) by proper statistical method (see below). We noticed a lag phase at short time / domain size that could be due to two effects: either small domains (less than ~100 monomers according to our analysis) cannot sever filaments or we did not see domains that severed rapidly, when they were still very small. The second hypothesis can be ruled out since we can detect domains much smaller than 100 mCherry-coflin-1 monomers (Figure S2C), and since severing events occurring away from detectable domains were negligible. The survival fraction was then fitted with an exponential, $f_{surv} = exp(-t.k_{sev})$, yielding the severing rate k_{sev}.

Depolymerization rate

To measure all depolymerization rates presented here we used our home-built Python algorithm. Given the background intensity and fluorescence of a typical filament (selected by the user), it searches for fluorescent objects appearing as actin filaments: the fluorescence of each pixel is at least 20% of that of the brightest pixel of the selected filament, the object is longitudinal and horizontal, not too short (e.g., fluorophore patches on the surface) or too long (e.g., several filaments aligned), etc.

Python then measures the fluorescence profile along the filamentous object and determines with subpixel resolution the position of the PE and BE as a decrease below 10% of the maximum intensity along the profile. A filament is then defined as a set of such objects, on different frames, with nearby anchoring points.

The user then selects correct filaments (not presenting artifacts coming either from the experiment or from the algorithm) and their length is fitted over time with a linear function to estimate the depolymerization rate.

Depolymerization of saturated filaments

All depolymerization rates were measured with unlabeled ADF/cofilin. To ensure that the filaments were saturated, we injected a solution of 1 to 2 μM ADF/cofilin at 50 mM KCl that quickly binds actin filaments.

Depolymerization of bare BE

When looking at bare actin BE, instead we tried to avoid the quick formation of domains and thus used a higher concentration of salt, 100 mM KCl [56]. Since ADF/cofilin in solution accelerate the depolymerization at BE while domains slow it down, it was clear when the BE would reach an ADF/cofilin domain. Only the early fast depolymerization was fitted and included into the rate calculation.

Polymerization rate

The polymerization of actin filaments in the presence of ADF/cofilin in solution was observed in TIRF, at typical frame rate 1f/30 s. We used the Python algorithm exactly in the same way as with depolymerizing filaments.

Capping rate

To estimate the binding rate of CP to polymerizing filaments we generated on ImageJ kymographs (*Reslice* function) of all filaments in a given region of interest. Any pausing event in the polymerization or depolymerization was accounted as a capping event as almost no pauses were observed in absence of CP. We then calculated the fraction of filaments that have been capped at least once (Figures 3I and 5C) and fit the data with a single exponential, $f_{CP} = 1 - exp(-t.k_{on,CP})$, where $k_{on,CP}$ is the binding rate of CP to the BE.

Uncapping rate

In the absence of ADF/cofilin, we estimated the uncapping rate of ADP-actin filaments in the absence of monomeric actin. Using kymographs on ImageJ, we calculated the fraction of capped BE over time (Figure 5D) and fitted the data with a simple exponential $f_{surv} = exp(-t.k_{off,CP})$, were $k_{off,CP}$ is the unbinding rate of CP.

To generate ADF-saturated filaments with a CP at their BE, we incubated for 1 min filaments with 1 μM ADF and 300 nM CP. Looking at kymographs indicated when CP was actually bound and stopped the depolymerization. We then switch to a solution with 1 μM ADF only and measured the fraction of non-depolymerizing filament. This fraction was fitted with the same function $f_{surv} = exp(-t.k_{off,CP})$.

Elongation of ADF/cofilin-saturated filaments

Saturated actin filaments can depolymerize for minutes even in the presence of ATP-G-actin (Figures 5E and 5F). To estimate the regrowth dynamics, we calculated the fraction of filaments that have been continuously depolymerizing and fitted with a simple exponential $f_{poly} = 1 - exp(-t.k_{on,actin})$, were $k_{on,actin}$ is the rate at which polymerization resumes.

Statistical method

In the course of an experiment, many filaments will be 'lost', for example because of severing, unwanted surface binding, light-induced pauses, etc. These events must be properly taken into account for the correctness of the analysis. We used the Kaplan-Meier method [57]. Briefly, survival fractions were calculated as follow:

$$f_{surv}(t=0) = 1,$$

$$f_{surv}(t+1) = \mathrm{f_{surv}}(t) * \frac{N_{t+1}}{N_{t+1} + n_{events,\ t+1}},$$

were $n_{events,\ t+1}$ is the number of filaments over which a studied event occurred (e.g., cofilin binding, pausing, repolymerization) between frames t and (t+1). N_{t+1} is the number of filaments on frame (t+1) that have not been lost and have not shown the studied event. Note that $N_t = N_{t+1} + n_{events,t+1} + n_{lost,t+1}$ where $n_{lost,t+1}$ is the number filaments lost between frames t and (t+1)

DATA AND SOFTWARE AVAILABILITY

Numerical simulations were written in C++ following a Gillespie algorithm [58], using Dev-C++ from Bloodshed Software.

Simulations of global experiments

We describe here the algorithm used to simulate global severing and depolymerizing experiments (Figure S4). The program source file is provided as a supplemental file (Data S1).

In order to compare our single-filament results to existing global measurements, we performed numerical simulations integrating all the reaction rates we have determined for domain nucleation, growth, and the depolymerization of filament ends (bare or ADF/saturated) in the absence of actin monomers. The program starts with a given filament population of ADP-actin filaments, in a fixed volume, with a total amount of cofilin in solution.

Each actin subunit can be in one of 8 possible states: bare PE, ADF/cofilin-saturated PE, bare BE, ADF/cofilin-saturated BE, bare F-actin, ADF/cofilin-occupied F-actin (boudary toward PE, boundary toward BE, or within domain). Each of these states corresponds to possible reactions, with rate constants that were determined in our single filament experiments. A ninth state would correspond to depolymerized actin monomers, which are removed from the system (they are assumed to be instantly sequestered) so that the G-actin concentration is always zero.

At each time step, the program computes the probabilty for each possible event: cofilin domain nucleation, cofilin domain growth, cofilin domain shrinkage, severing at either type of domain boundary, BE end depolymerization (either a bare or a saturated BE), PE (either a bare or a saturated PE). Departure of ADF/cofilin from within a domain is considered negligible. These probabilities depend on the rate constants of each reaction (which were determined in our study, see Figures 1, 2, 3, and 4), on the free cofilin concentration and on the number of available reaction sites.

Based on these probabilities, the program randomly determines when the next event takes place, what type of event it is, and on which site it takes place. The filament population and the cofilin concentration are then modified accordingly.

Knowing the fraction of F-actin subunits that are bound to ADF/cofilin over time, an 85% quenching of the pyrene signal upon ADF/cofilin binding [24] can also be taken into account.

Simulations of elongating populations

We describe here the algorithm used to simulate the outcome of elongating filament populations exposed to actin, ADF/cofilin and CP (Figures 6 and S7). The program source file is provided as a supplemental file (Data S2).

Following a similar Gillespie algorithm, we tracked a population of filament barbed ends over time, exposed to constant concentrations of monomeric actin, ADF/cofilin and CP. Each BE is in one of four states: (i) non-capped and with a bare (no ADF/cofilin) barbed end region; (ii) capped with a bare (no ADF/cofilin) barbed end region; (iii) capped with an ADF/cofilin-decorated region; and (iv) non-capped with an ADF/cofilin-decorated region. In each state, the BE is growing (i), paused (ii), paused (iii) and depolymerizing (iv). Initially, every BE is growing in state (i). All the transitions from one state to another are simulated using rate constants determined experimetally: capping/ uncapping bare and ADF/cofilin-decorated BE (Figures 5C and 5D), ADF/cofilin decorating a capped BE (Figure S7A), and rescues of depolymerizing BE (Figure 5F). The transition from (i) to (iv), i.e., directly switching from elongation to depolymerization without being capped, is neglected. The transition from (iii) to (ii) is prevented by the presence of ADF/cofilin in solution. Severing events are not considered.